Irish Ice Sheet dynamics during deglaciation of the central Irish Midlands: Evidence of ice streaming and surging from airborne LiDAR

Catherine A. Delaney*, School of Science and the Environment, Manchester Metropolitan University, John Dalton East, Chester St., Manchester M1 5GD.

Stephen McCarron, Maynooth University Dept. of Geography, Rep. of Ireland.

Stephen Davis, School of Archaeology, University College, Dublin, Rep. of Ireland.

*Corresponding author. Tel: +44 161 2471567; Email: c.delaney@mmu.ac.uk

Abstract

High resolution digital terrain models (DTMs) generated from airborne LiDAR data and supplemented by field evidence are used to map glacial landform assemblages dating from the last glaciation (Midlandian glaciation; OI stages 2-3) in the central Irish Midlands. The DTMs reveal previously unrecognised low-amplitude landforms, including crevasse-squeeze ridges and mega-scale glacial lineations overprinted by conduit fills leading to ice-marginal subaqueous deposits. We interpret this landform assemblage as evidence for surging behaviour during ice recession. The data indicate that two separate phases of accelerated ice flow were followed by ice sheet stagnation during overall deglaciation. The second surge event was followed by a subglacial outburst flood, forming an intricate esker and crevasse-fill network. The data provide the first clear evidence that ice flow direction was eastward along the eastern watershed of the Shannon River basin, at odds with previous models, and raise the possibility that an ice stream existed in this area. Our work

demonstrates the potential for airborne LiDAR surveys to produce detailed paleoglaciological reconstructions and to enhance our understanding of complex palaeo-ice sheet dynamics.

Keywords: LiDAR; Ireland; crevasse-squeeze ridges; ice surging

1. Introduction

Airborne LiDAR (Light Detection and Ranging) surveying allows the remote sensing of earth surface topography at unprecedented high spatial resolutions (<1 m horizontal resolutions and vertical resolutions of <0.25 m). This allows the relatively swift identification and precise measurement of archaeological and geomorphological features at a higher level of detail and accuracy than that achieved by traditional field study methodologies (Slatton et al., 2007; Roering et al., 2013).

In paleoglaciology, digital terrain models (DTMs) of >20 m horizontal resolution generated from satellite radar surveying have been central in the mapping of ice sheet subglacial bedforms and reconstructing the changing dynamics of ice sheets(e.g., Clark, 1993; McCabe et al., 1998; Greenwood and Clark, 2009a; Clark et al., 2012; Hughes et al., 2016). In Ireland, DTMs generated from radar, aerial photos, and satellite images have been used to map subglacial bedforms from the last Irish Ice Sheet (IIS) (Midlandian; OI stage 2-3; McCabe et al., 1998; Knight et al., 1999; Clark and Meehan, 2001; Greenwood and Clark, 2008). This approach has been used to infer bedform 'flowsets' (Clark and Meehan, 2001; Greenwood and Clark, 2008, 2009a) related to ice sheet flow phases and thus reconstruct ice dynamics where bedforms (e.g., drumlins) and contemporaneous ice marginal positions (e.g., terminal moraines) are well preserved.

Very low-amplitude features (<1 m high) are unlikely to be recognised on radar data or photographs, especially if they have poorly defined slope breaks (Smith et al., 2006). This category of topography includes gently undulating and low-amplitude hummocky terrain, which commonly

occurs in marginal zones of former ice sheets and is widespread across the Irish Midlands (Synge and Stephens, 1960; Synge, 1979; Warren, 1992; Meehan, 1999; Delaney, 2001). However, the evidence is increasing that higher resolution spatial data can significantly improve the detection of large- and small-scale glacial features, improving the accuracy of landform interpretation (e.g., Cline et al., 2015; Dowling et al., 2015). Small-scale features — including controlled and uncontrolled hummocky terrain, ice-flow transverse ridges, and crevasse squeeze ridges — often record critical changes in ice sheet dynamics at the time of formation, including in basal thermal regime, ice flow velocity and direction, and ice marginal readvances (e.g., Eyles et al., 1999; Evans et al., 2008; Ottesen et al., 2008; Evans, 2009; Andreasson et al., 2014). Recent evaluations of high-resolution multibeam acoustic surveys in offshore areas and airborne LiDAR onshore indicate that such features are critical to understanding evolving ice dynamics during overall ice sheet recession during glacial terminations (e.g., Andreasson et al., 2014; Bjarnadóttir et al., 2014; Cline et al., 2015; Möller and Dowling, 2015).

In this study we use two high-resolution DTMs generated from airborne LiDAR data to map the glacial geomorphology of two nearby areas in the central Irish Midlands. The mapping is supplemented by field investigations of sediment exposures, producing morphosedimentary evidence of glacial events in the region during the last glaciation. The evidence is used to generate new palaeoglaciological models of ice sheet dynamics in a region where previous interpretations of ice sheet dynamics have been based almost entirely on the large-scale pattern of glaciofluvial evidence.

2. Regional setting

2.1. Regional geology and topography

The central Irish Midlands consists of a low-relief plain (~40-70 MOD, meters above ordnance datum), drained by the River Shannon and its tributaries (Fig. 1). The plain is underlain by Carboniferous limestones, with inliers of Paleozoic sandstones and siltstones (Sevastopulo and Wyse-Jackson, 2009). The area is poorly drained but tilts generally westward from a watershed at

77 ~80 MOD, ~12 km east of Tullamore, County Offaly, to ~37 MOD at the River Shannon. The plain is
78 defined to the south by the rising topography of the Slieve Bloom Mountains (480-514 MOD) and to
79 the north and east by gently rising, NE-SW striking (bedrock controlled) topography.
80
81 *2.2. Regional glacial landform distributions*
82 The distribution of larger glacial landforms dating from the last (Midlandian) glaciation across
83 the Irish Midlands is well documented (e.g., Sollas, 1896; Synge and Stephens, 1960; Synge, 1979).
84 The dominant glacigenic landforms in the study area are well developed (≤60 m high and up to 40
85 km in length) west- to east-trending eskers (Fig. 1; Sollas, 1896; Farrington with Synge, 1970; Warren
86 and Ashley, 1994; Pellicer et al., 2012). Smaller SE-trending eskers occur along the northern margin
87 of the basin (Delaney, 2001a,b, 2002), and short SE-aligned segments also occur within the west- to
88 east-trending esker group (Gallagher et al., 1996). Moraines are rare in the area, and
89 reconstructions of ice marginal positions through time are based primarily on the occurrence of ice-
90 contact deltas and subaqueous outwash fans at the downstream ends of esker conduit deposits,
91 together with some minor, short moraines (Delaney, 2001a,b, 2002; Pellicer et al., 2012). Drumlins
92 and mega-scale glacial lineations (MSGLs) occur on the higher ground around the basin margins but
93 are rare on lower ground (Greenwood and Clark, 2008, 2009a; Fig. 2A). Inter-esker areas are partly
94 covered by glaciolacustrine deposits, overlain by Holocene peat and alluvium, thought to have been
95 deposited in a topographically controlled, proglacial, ice-contact lake (Paleolake Riada). This lake
96 formed as ice receded westward and downslope during deglaciation and was dammed by ice to the
97 west and northwest and by rising topography to the north, east, and south. At its maximum extent
98 the lake drained through a col at 82 MOD, 10 km east of Tullamore. This is also the height of many
99 ice-contact deltas around the lake basin, indicating a relatively stable lake surface level (Delaney,
100 2002, 2007; Pellicer et al., 2012). Further recession of ice westward is presumed to have allowed
101 drainage of the lake southward around the western margin of the Slieve Bloom uplands.

Between the glaciolacustrine basins, flat, undulating, and hummocky terrain is underlain by a mix of glaciofluvial sand and gravel deposits and sandy-silt and silty-clay diamicton, both rich in limestone (Pellicer et al., 2012). Diamicton thicknesses, where known, are generally 1-10 m; and hummocky terrain is particularly concentrated around the northern and western margins of the basin but also occurs in other areas around the eskers (Fig. 1; GSI, 2016).

(FIGURE 1 HERE)

2.3 Regional palaeoglaciological models

The absence of widespread indicators of active ice flow, together with the dominance of glaciofluvial sediments, means that the glacial morphosedimentary sequence in this area has been interpreted as a deglaciation landscape, formed by ice recession and sedimentation into an expanding ice marginal lake (Pellicer et al., 2012). This absence of evidence for active ice flow has led to contestation over the interpretation of ice recession direction (Fig. 2). Warren and others (Warren, 1992; Warren and Ashley, 1994; Pellicer et al., 2012) have used water palaeoflow directions, constructed from subglacial esker and ice-marginal kame sediments, to suggest that the esker Riada and the Ballyduff esker formed contemporaneously in an interdomal position. This model requires an ice dispersal centre to the southwest feeding ice northeastward, and a second dispersal centre to the northwest feeding ice flow southeastward (Fig. 2B). An alternative multiphase model, involving ice flow eastward and initial recession westward, followed by readvance from the north has also been proposed (Synge, 1952; Delaney, 2002; McCabe, 2007). Mapping of subglacial lineations in the area by Greenwood et al. (2009a, b) has failed to resolve this issue (Fig. 2A), which is of critical importance in the construction of regional palaeoglacological models (cf Warren et al., 1992).

(FIGURE 2 HERE)

3. Methods

LiDAR data acquired during 2011 for flood risk assessment and infrastructure planning were obtained for three areas in the Irish Midlands. For areas 1 and 3 (see below), the data were processed to remove survey artefacts, vegetation cover (using the last return of the laser survey signal), and anthropogenic structures; and the resulting point cloud data was used to interpolate DTM rasters for each area of a nominal 0.5-1 m horizontal and 0.12-0.25 m vertical resolution. For area 2, the data had been previously processed in a similar manner and was already in raster format.

The DTM rasters were relief-shaded using the Relief Visualisation Toolbox application, a programme originally developed for archaeological surveys (Kokalj et al., 2011; Zakšek et al., 2011). Relief-shaded terrain models were generated using the multidirectional shading tool, which composites relief-shade models lit from 16 different azimuths. Incident light elevation angle was set between 20 and 25°, with a vertical exaggeration of up to x4 applied to exaggerate low-amplitude features. In addition, where landforms were particularly faint, a principal component analysis (PCA) of the original hillshaded image was undertaken. This procedure shows the three main components of the image only and minimises noise (Kokalj et al., 2011). Landforms in areas immediately outside the DTM footprints were mapped where appropriate, using a combination of stereo pair and single vertical aerial photos.

Mapping of candidate glacial landforms from DTMs was field checked and supplemented by field surveying. During field surveying, available sedimentary exposures were photographed and logged; and fabric data on clast orientations in diamictons were obtained where appropriate.

4. Results

4.1 Area 1: Tullamore

The LiDAR DTM covers a low-relief (54-82 MOD), trapezoid area of 13 km by 5 km around the Tullamore River, centred on Tullamore town (Figs. 1, 3). About 9 km^2 of the central part of the area is urbanised, and construction has resulted in some landscape alteration and the removal of small-

scale landforms. At its margins, the data patch clips the southern flank of the Ballyduff esker to the north and the Blackwood ice-contact delta-kame (Pellicer et al., 2012) to the southwest.

Warren and Ashley (1994) suggested that the area was covered by ice feeding from an ice dome to the southwest and interpreted ice flow direction as northeast. However, Farrington (with Synge, 1970) and Warren (1987) identified small moraines in the area, which indicate ice recession was west to southwest, implying ice flow was roughly eastward, but deflected northward around the Slieve Bloom mountains. More recently, the GSI have mapped drumlins trending southeast across the area (GSI, 2016; Fig. 1).

(FIGURE 3 HERE)

The following glacial features were identified on the LiDAR DTM.

4.1.1. Lineations

Multiple (<10) low-amplitude, highly elongate, streamlined ridges with subparallel long axes and associated grooves trend eastward (average bearing 083°) across Area 1 (Figs. 3, 4, 5). Smooth ridges crests are between 0.3 and 4 m higher (average height 0.98 m) than surrounding terrain, with ridge widths between 50 and 116 m and measured lengths of 1.9-4.7 km. Some ridges show abrupt truncation or extend beyond the DTM coverage, so maximum ridge length is greater. Minimum elongation ratios are >1:30. Five ridges with well-defined, wider, rounded western ends are visible in the eastern part of area 1, and additional traces of lineations in the form of grooves are also visible in places (Figs. 3, 4, 5). Two ridges in the north of the study area extend eastward from a protuberance (Fig. 3A); however, the two most southerly ridges are unrelated to any prominent bedrock irregularities and have subtle seeding points, widening over 500 m to their maximum width and height before tapering out gradually eastward (Fig. 5). Judging by the occurrence of faint linear traces on aerial photos, the ridges and grooves appear to form part of a larger group of these features that continues eastward.

(FIGURES 4 AND 5 HERE)

178 A roadside exposure measuring ~1 m high by 10 m long crosses one well-developed lineation
179 orthogonally (X on Fig. 3A) and shows one lithofacies, a limestone clast-rich diamicton with a pale
180 yellow, silty matrix (Fig. 6A). The diamicton contains fractured clasts with angular clast slabs off-
181 lapping each other on centimeter-scales progressively upward to ~85° (Fig. 6B).
182 *(FIGURE 6 HERE)*
183 *Interpretation:* The consistent ridge long-axis azimuth indicates formation under a persistent
184 and strong controlling mechanism. The low-amplitude, highly streamlined elongate morphology and
185 the occurrence of a tectonically deformed diamicton, with sheared clasts indicating a high normal
186 confining stress and shear stress applied in the direction of ridge long axes, both indicate
187 modification of a diamicton in a highly stressed, confined environment. The ridges and
188 accompanying grooves are interpreted to form part of west- to east-trending mega-scale glacial
189 lineations (MSGLs). The precise mechanism of formation of MSGLs is debated; however, the
190 landforms are thought to form from a combination of erosion, transfer, and deposition of diamicton
191 in a deforming subglacial bed, in association with accelerated ice flow (Ó Cofaigh et al., 2013). These
192 features are discussed further below.
193
194 *4.1.2. Cross-cutting ridge sets*
195 Overlapping sets of low-amplitude ridges occur over large parts of the study area.
196 Preservation of the ridges is partial, but where best preserved they form a rectilinear pattern (Figs.
197 4, 5).
198 Three ridge orientations can be identified on the LiDAR DTMs. The most prominent ridge set
199 (ridge group A) are aligned N-S to NNW-SSE (mean alignment 343-163°) and were partly mapped by
200 Farrington with Synge (1970) and Warren (1987). The ridges are arranged in an east-west oriented
201 belt, with further ridges detectable on aerial photos up to 4 km to the east, but not north or south of
202 the DTM area. Group A ridges have rounded or slightly flattened crests, with sideslope angles of
203 <25°, are between 300 and900 m long (average length 558 m; aligned segments traceable for up to

2500 m), up to 8 m high, and between 40 and 100 m wide. Ridge crestlines are increasingly broken westward. Spacing between ridges is between 53 and 157 m, with an average spacing of 112 m (Fig. 3C). Ridges are generally straight, becoming slightly arcuate (convex to the east) along the southern margin of the group. Minor exposures indicate that the ridges are composed of diamicton. A 4-m-long trench cut in undulating terrain at the western limit of the ridge distribution (Y on Fig. 3A (Irish National Grid (ING) 229813, 225513; UTM 596368m E 904157m N) is shown in Fig. 7. A basal matrix-poor boulder breccia, containing angular and often fractured limestone clasts (facies A) and presumed close to bedrock, is overlain by a crudely stratified, highly consolidated, matrix-rich, grey-pale brown diamicton (facies B). Clasts are pebble to boulder-sized, subangular to subrounded, occasionally striated and include pale and dark blue limestones (>90%) and yellow sandstones (<10%). Clasts exhibit a well-developed, bimodal orientation. The uppermost facies (C) consists of massive, yellow sandy silts with sparse, generally boulder-sized clasts of angular pale limestones.

(FIGURE 7 HERE)

A second set of ridges aligned at 017-197° (ridge group B) overlies the group A ridges, forming a partially preserved rectilinear grid in this area (Figs. 4, 5). Group B ridges are shorter than group A types (mean length 227 m), lower (heights <5 m) and narrower (20-30 m width), and have less clearly defined basal slope breaks. A third group of ridges aligned at 127-307° (group C) occur throughout the area. These have a mean length of 189 m, are under 5 m high and are 30 m wide.

The ridges do not appear to have been deposited in a distinct chronological sequence. Where ridges intersect, a groove is often visible in the underlying ridge, indicating reworking of material from the lower ridge (arrows on Fig. 4, 5). No consistent pattern of reworking occurs — for example, in Fig. 4, group A ridges overlie (X on Fig. 4) and are overlain by Group B ridges (Y on Fig. 4).

Interpretation: Small transverse ridges are very common in glaciated terrain and form in a number of ways, including annual and subannual, ice-marginal push and squeeze ridges (Price, 1970; Sharp, 1984; Kruger, 1994; Evans and Hiemstra, 2005); controlled moraine formed by supraglacial meltout of debris-rich bands within the ice margin (e.g., Evans, 2009); and subglacially, either as

crevasse-squeeze ridges (CSRs) formed in flow-transverse crevasses (including washboard moraine, e.g., Cline et al., 2015) or as ribbed moraine formed of meltout till and linked to a thermal transition from warm- to cold-based ice within the ice sheet (e.g., Möller and Dowling, 2015).

Any interpretation must explain two features: firstly no evidence of reshaping of the ridges by active ice flow is visible, as expected if overriding had occurred; and secondly group A ridges appear to overlie and underlie group B and C ridges. One possibility is that the lower transverse ridges were formed ice-marginally as push and squeeze ridges (Price, 1970; Sharp, 1984; Kruger, 1994; Evans and Hiemstra, 2005). However, if this was the case, a readvance of ice across the ridges would be necessary to form the overlying oblique ridges, a process that normally involves fluting and reworking of material to form asymmetric ridge profiles and arcuate planforms, features not seen in the flow-transverse ridges (Sharp, 1984; Benn and Evans, 2012). Formation as controlled moraine by supraglacial meltout of debris-rich bands within the ice margin (Evans, 2009) is also discounted, as again, reworking into upper ridges would not be possible without readvance and reshaping.

Instead, formation of the entire ridge network subglacially is preferred and is supported by the diamictic composition of the ridges and well-developed fabric. Two possibilities exist. The first possibility, formation as ribbed moraine formed of meltout till and linked to a thermal transition from warm- to cold-based ice within the ice sheet (e.g., Möller and Dowling, 2015) is again unlikely, as such ridges are usually strongly asymmetric and laterally variable in profile because of fluting of the surface.

Instead, we consider formation as crevasse-squeeze ridges (CSRs; Sharp, 1985) to be the most likely mechanism for all the ridge sets, with formation of the three different ridge orientations taking place near-concurrently but after formation of the underlying MSGLs. Crevasse-squeeze ridges forming geometrical networks were originally identified in front of modern surging glaciers and are considered a diagnostic feature of ice stagnation after a period of accelerated, extensional ice flow (Sharp, 1985; Evans and Rea, 1999, 2003; Evans et al., 2007). The CSRs are thought to form by the injection of wet basal sediments upward into extensional crevasses, under high basal water

256 pressures (Sharp, 1985; Rea and Evans, 2011). Similar rectilinear ridge networks have been
257 observed on the beds of modern and Quaternary temperate and polythermal glaciers and are
258 associated with surging glaciers and ice streams in onshore and offshore situations (Boulton et al.,
259 1996; Ottesen et al., 2008; Ó Cofaigh et al., 2010; Andreasson et al., 2014; Jónsson et al., 2014; Evans
260 et al., 2014, 2016; Cline et al., 2015; Flink et al., 2017). Ice-flow transverse (set 1) ridges in area 1 are
261 somewhat larger than usual; however, similar larger transverse ridges have been observed in front
262 of modern surging glaciers in Svalbard (Boulton et al., 1996; Flink et al., 2017) and on the bed of
263 former ice streams (Evans et al., 2016).
264
265 *4.2. Areas 2 and 3: Birr*
266 These areas are located in the southwest of the study area around Birr, in a low-relief area
267 around the Little Brosna and Ballinurig rivers, which drain WNW toward the Shannon River. The
268 available high resolution LiDAR data cover an irregularly shaped polygon (~59 km^2) north of Birr
269 (area 2; Figs. 1, 8, 9) and a 2 km^2 square west of Birr (area 3; Figs. 1, 10). Both areas have a low relief
270 range (between 40-60 MOD, excluding prominent esker ridges). Surfaces in this area below 50 MOD
271 are characterised by raised bog, reclaimed bog, and alluvial floodplain, while glacial features form
272 the areas above 50 MOD.
273 *(FIGURE 8 HERE)*
274 *(FIGURE 9 HERE)*
275 Previous studies have identified a complex of glaciofluvial ridges oriented west to east and
276 southwest to northeast (Gallagher et al., 1996; Greenwood and Clark, 2009a; GSI, 2016; Fig. 1), with
277 a set of NNW-SSE–oriented ridges interpreted as recessional moraines by Gallagher et al. (1996).
278 The glaciofluvial ridges have been interpreted as conduit fills (eskers) leading to subaqueous ice-
279 marginal deposits formed in a proglacial, ice contact lake, with changing esker orientation reflecting
280 deflection of an eastward-flowing ice sheet around the Slieve Bloom massif to the southeast
281 (Gallagher et al., 1996). Hummocky terrain is present around the eskers and has been mapped as

either hummocky sand and gravel or as underlain by limestone till (GSI, 2016). Drumlins and MSGLs have been mapped to the west and northwest of both areas (Fig. 1).

(FIGURE 10 HERE)

The following glacial features were identified on the LiDAR DTMS.

4.2.1. Lineations

Elongate, closely spaced ridges and grooves trending at 307-127° similar to those seen in area 1 are visible in the northern part of area 2 (Figs. 8, 9, 11) and are interpreted as MSGLs. Ridges have similar heights and widths to those in area 1 but are shorter, between 700 and 1600 m (average 1055 m) in length, with an elongation ratio of >1:13. However, they are partly truncated and overlain by hummocky terrain to the south, so original lengths are likely to have been greater. No good exposures were found, but drilling by the Geological Survey of Ireland has enabled mapping of the area as 'limestone till'.

(FIGURE 11 HERE)

Two drumlins were also identified (Figs. 8, 9, 11). One immediately NW of the MSGLs has been mapped by the GSI and Greenwood et al. (2008) within an area of limestone till; a second along the southern margin of the DTM was mapped by the GSI (2016) as a sand and gravel deposit but has a fluted surface.

4.2.2. Hummocky terrain

Hummocky terrain (HT) occurs as 1-2 km^2 patches in area 2 and covers all of area 3 (Figs. 8, 10). These areas have been mapped previously by the Geological Survey of Ireland (GSI 2016). We classify HT into three main types on the basis of morphological characteristics visible on the LiDAR DTMs.

Hummock terrain type 1 (HT1): HT1 is present in the northern part of area 2 (Figs. 8, 9, 12A,B), immediately downstream of the MSGLs, and throughout area 3 (Fig. 10). It is confined to

higher ground and appears to have been partly eroded by post-glacial fluvial action. The HT1 consists of ridges and mounds <5 m high, with rounded or flattened crests, and with intervening hollows and grooves. Mounds and ridges and grooves exhibit preferred orientations.

Where HT1 occurs in area 2 two prominent ridge and groove orientations are visible (320-140° and 235-055°) with two minor orientations at 275-095° and 350-170° (Figs. 12A,B; 13A,B). Truncation of ridges by grooves indicates that the oldest orientation is at 320-140°, parallel to MSGLs to the north (shown in Fig. 11), and these features are interpreted as remnants of MSGLs; they are round crested and relatively wide (>50 m), with height differences between crest and trough of between 0.8 and 1.5 m. Of the remaining ridges and grooves, the largest group is aligned transverse to the MSGLs, at 235-055°. Larger ridges in this group (height 2-4 m; width 40-120 m) have flattened tops, well-defined basal slopes, and are steeper on the distal (downice) side; smaller ridges are narrower, lower and near-symmetrical. Minor exposures indicate that the ridges are underlain by diamicton containing fractured clasts, but with no evidence of directional shearing. All ridges vary in width and height along their length. A third ridge alignment at 350-170° appears in places to have formed from reshaping of the flow-transverse ridges into flutes. The final orientation is dominated by grooves oriented at 275-095° that truncate other ridge and groove orientations.

Area 3 has a similar pattern, with MSGL remnants aligned at 305-125° overlain by a set of closely spaced ridges aligned at right angles (215-035°; Figs. 10A, B). As in area 2, morphology varies with size, and some fluting has occurred. Two further ridges aligned at 0-180° in the northern part of the DTM are 70-120 m long, up to 6 m high, with well-defined basal slope breaks and sharp-crested and flattened tops.

(FIGURE 12 HERE)

Hummocky terrain type 2 (HT2): This type of hummocky terrain is visible in area 2 (Figs. 12C,D; 13C,D). It contains features in common with HT1 topography, i.e., is primarily formed from MSGL remnants overlain by transverse ridges at similar orientations to those seen in HT1 topography in area 2. In addition, higher, sharp-crested ridges with slightly sinuous crests also occur

and are interpreted as remnants of conduit fills (eskers). The principal difference from HT1 is the presence of discontinuous, anastomosing channels cut into the hummocky surface (Figs. 12C,D). These are commonly flat-bottomed with steep sides and undulating long profiles that rises southeastward. They are interpreted as subglacial meltwater channels.

(FIGURE 13 HERE)

Hummocky terrain type 3 (HT3): This type of hummocky terrain is present in the southern part of area 2 (Figs. 12E,F) and is mapped as hummocky sand and gravel by the GSI (2016). It is bounded by eskers to the west, south, and east (GSI, 2016). The HT3 consists of multiple, short, sinuous ridges forming an interconnected network. These ridges have been partly anthropogenically modified, but the overall pattern of ridges is preserved. The dominant ridge orientation is 335-155°, parallel to the eskers to the east and west, and subparallel to the MSGLs to the north. Shorter, sharp-crested, 1-7 m high discontinuous sections with well-defined basal slopes and exhibiting low sinuosity oriented at 235-055° are also present. Traces of a third, NE-SW–oriented set of straight ridge segments can be detected underlying the sinuous ridge set. The ridges are similar in appearance to conduit fill eskers.

Interpretation: We consider the varieties of hummocky terrain seen here to be multigenetic in origin, involving subglacial squeezing of wet sediments and subsequent glaciofluvial erosion and sedimentation. The HT1 and HT2 are interpreted as a continuum of subglacial landforms, formed under soft bed conditions but under varying ice flow regimes. The MSGLs indicate accelerated ice flow southeastward across the area. They have been partly eroded during emplacement of the overlying ridges. The overlying flow-transverse ridges have an asymmetrical cross-profile and may have originated as ice-marginal features. However, the presence of fluting, grooves, and oblique superimposition of further ridges supports a subglacial origin; and we consider HT1 and HT2 to have formed as CSRs, i.e., by the subglacial squeezing of wet basal sediment into tensional crevasses, in a

similar manner to the ridges in area 1. In areas 2 and 3 the relatively poor preservation of MSGLs is considered the result of a more aggressive reworking of sediment into closely spaced crevasses, and the further overprinting of ridge sets because of to the continuation of active ice flow during formation of the overlying ridges and grooves. This characteristic is shared with ribbed moraine described by Möller and Dowling (2015). In addition, HT2 appears to have been eroded subsequently by channelized subglacial meltwater flow in Nye-channels, with channels cut generally subparallel to local esker azimuths (see below).

The HT3 differs in form to HT1 and HT2 but also contains evidence for channelized meltwater flow within the ice sheet. The area is underlain by sand and gravel (GSI, 2016), and the sinuosity and composition of the larger ridges in this area, together with links to adjacent eskers, indicates that these are also ice-walled conduit or channel fills. We consider the alignment of the sinuous ridges and the occurrence of linear ridges and grooves within HT3 to indicate formation within crevasses, either supraglacially or subglacially. Similar ridge networks have been described at modern glaciers where subglacial water has been diverted into crevasses within a fractured snout (Roberts et al., 2000; Russell et al., 2006; Bennett et al., 2000; Evans et al., 2012) and in Quaternary eskers in Finland (Mäkinen and Palmu, 2008). The modern analogues formed during glacial outburst floods as discharge increased rapidly, beyond preexisting conduit capacity, and are often associated with hydrofracturing of adjacent crevasses. This is discussed further below.

4.2.3. Eskers and kames

Eskers and associated kames are the dominant landform in area 2 (Figs. 1, 8, 9). Previous mapping in the area southeast of the study area (Gallagher et al., 1996; GSI, 2016) has identified a major esker, the Kilcormac esker (A on Fig. 8). The esker undergoes a number of minor high angle changes in direction before changing orientation sharply from WNW-ESE to SW-NE (Figs. 8, 9). Geological Survey of Ireland mapping (2016) also identified a short tributary (A1) that feeds in to its northern flank just before a sharp (60°) reorientation. A distributary (A2) is also visible, leading

386 eastward from the main ridge. A second esker (B on Fig. 8) runs southeastward across the centre of
387 the study area, parallel with tributary A1, terminating close to the point where A1 joins A. Esker B
388 also appears to have a tributary, B1, which joins the main ridge close to the terminus. Further esker
389 segments lie immediately south of esker A.

390 The LiDAR DTM, combined with sedimentological evidence, provides considerable extra
391 information on the nature and distribution of glaciofluvial sediments in the Birr area. Glaciofluvial
392 ridges are more extensive than previously thought and converge in the south of the area covered by
393 the DTM (Fig. 8). The eskers mapped generally are narrow and steep sided with a well-defined basal
394 slope break, but with some variation in width and height occurs along the length of individual ridges
395 (from <10 m high with widths of 25-70 m, to 10-18 m high with widths of 80-120 m). Exposures in
396 the larger ridges indicate that they are underlain by horizontal- and cross-bedded boulder to sand-
397 sized sediments indicating transport parallel to the ridge long axis (Fig. 14A). Sediments become
398 increasingly organised downstream (southeast and eastward), with a transition from matrix-rich to
399 dominantly bimodal sediment distributions with a corresponding transition from internally massive
400 to well-bedded gravels. Sandy, cross- and ripple-laminated beds increase in frequency downstream,
401 indicating a transition from high energy, episodic, sediment-laden, often hyperconcentrated flood
402 flows to fully Newtonian flows with variable current strengths, typical of glaciofluvial environments
403 (e.g., Brennand, 1994; Delaney, 2001a, 2002). This morphology and sedimentology is characteristic
404 of conduit fills (Brennand, 2000; Perkins et al., 2016), and these sediments are interpreted as such.
405 Faulting at the sides of ridges has occurred, but the sediments at the ridge core are undisturbed,
406 indicating a probable subglacial origin for the conduits.

407 *(FIGURE 14 HERE)*

408 Wider, equally elevated areas (>40 m width) have a less well-defined basal slope. Along
409 esker A, a wider area at the western (upstream) end is clearly flat-topped and has multiple adjoining
410 short ridges extending northward (Fig. 15A). Exposures indicate this is a truncated surface, and
411 beach deposits occur along the esker flanks (Fig. 14B). The flat top and short ridges are likely to have

originated from erosion and reworking by wave action in Paleolake Riada. Wider areas at the downstream end of eskers B and B1 are underlain by horizontally bedded cobble and pebble gravels and by cross-bedded and ripple-laminated coarse to fine sands, with interbeds of ripple and drape-laminated fine sand, silt, and clays, indicating subaqueous deposition (Figs. 14C,D). These are interpreted as subaqueous outwash fan deposits.

(FIGURE 15 HERE)

Previously unidentified eskers in the area are distinguished using the LiDAR-generated DTMs. The eskers trend southeastward and eastward. Esker B1 is distinguishable as an entirely separate ridge, running parallel to esker B. Newly identified southeastward-trending eskers include esker C to the SW of esker A (previously interpreted as hummocky sandy and gravel and two short ridges (D, E) immediately west of a major NW-SE to SW-NE change in the direction of esker A (Fig. 8). Ridges D and E cross an eastward-trending glaciofluvial ridge (F) that runs subparallel to the minor eastward-aligned section of esker A to the north (Figs. 8, 15B). Ridges D and E clearly overlie F, almost orthogonally, although the path of ridge D deflects along the top of ridge F for a circa 50 m (Fig. 15B). Additional eastward trending ridges can be seen to the east of esker A (A2 on Fig. 8), in the direction of a large isolated kame. Fragments of these ridges are also traceable to the west of esker A, subparallel to shorter ridge segments within the HT3 zone in this area (H on Fig. 8).

Previously unidentified ridges northwest of esker B appear to lead toward the western upstream end of the esker and are interpreted as the infills of tributary conduits (B2 and B3 on Fig. 8).

Interpretation: Eskers in area 2 are interpreted as conduit and channel fills, with wider areas underlain by ice-marginal point discharges from conduits/channels or conduit/channel sediments reworked as pro-glacial lake shoreline deposits. Larger eskers appear to be subglacial, but smaller eskers and sinuous ridges within HT3 are less continuous and may be partly fills of en- or supra-glacial conduits and channels. This network of conduits and channels exhibit two distinctive features. First, channels and conduits have two distinct, near orthogonal alignments: southeastward

and east-northeastward. The SE alignment dominates in the northern part of area 2 and is subparallel to subjacent subglacial lineations, and we interpret this as reflecting control by the ice sheet surface slope upon hydraulic potential within the ice mass. To the south, ENE-aligned ridges become more common. In places, these connect directly with southeastward-aligned esker segments, and these eastnortheast-aligned sections are interpreted as a consequence of meltwater routing along a set of eastnortheast-aligned crevasses in the ice sheet. However, one of these eastnortheast-oriented ridges, esker A, continues eastnortheast for a considerable distance outside area 2, paralleling other Midlands eskers, indicating that ice sheet surface slope was also a factor in orientation. In addition, some ENE-aligned ridges underlie southeastward-aligned ridges, suggesting that they partly predate the southeastward-aligned landforms and suggesting a major reorganisation of the subglacial drainage network, from an east-northeastward-draining to a southeastward-draining system. We consider this reorganisation to have accompanied a southeast-directed ice marginal readvance, which also partly removed eastnortheast-trending conduit fills by subglacial erosion. Readvance was followed by the emplacement of sediment along new conduits draining southeastward toward an ice margin striking approximately northeast-southwest, beyond the area of the DTM.

A second significant feature is that the eskers indicate the occurrence of many closely spaced, converging conduits, suggesting concentration of flow in a topographic low. This differs from conduit spacing that develops under normal meltwater fluxes in modern systems, where conduits are usually regularly spaced along the ice margin (Boulton et al., 2007; Storrar et al., 2014). The routing of subglacial meltwater through closely spaced subglacial and englacial conduits and into connecting crevasses as indicated by the adjacent HT3 zone is associated with subglacial outburst floods (Roberts et al., 2000; Russell et al., 2006; Bennett et al., 2000; Evans et al., 2012). This is discussed further below.

5. Discussion

464 The suite of low-amplitude landforms visible on high-resolution DTMs provides critical new
465 evidence for elucidating ice sheet events during overall deglaciation of the Irish Midlands. When
466 combined with the palaeohydrological information provided by regional glaciofluvial features,
467 changing ice sheet dynamics, ice flow directions, and surface slope directions can be reconstructed
468 to construct a temporal sequence of ice sheet reorganisation events. We identify evidence for five
469 major stages in the development of the late Midlandian ice sheet during deglaciation of the central
470 Midlands (Fig. 16).
471 *(FIGURE 16 HERE)*
472 *Stage 1:* The oldest glacial landforms identified are the MSGLs in area 1, as these underlie
473 other landforms in the area (Fig. 16). The MSGLs are characteristic of ice streams and surging glacier
474 beds (Clark, 1993; Stokes and Clark, 2001) and provide clear evidence of wet-bedded, accelerated ice
475 flow involving bed deformation across the central Midlands plain trending eastward. Where full
476 lengths are traceable in area 1, MSGLs are close to maximum elongation values measured for these
477 landforms under modern and former ice streams (Spagnolo et al., 2014). A comparison of Irish
478 Midland MSGL parameters to known ice stream examples indicates that the Irish Midland MSGLS
479 are likely to have formed under conditions of low basal shear stress (<10kPa), under relatively thin
480 ice (<650 m) at velocities in excess of 900 m a^{-1} (Jamieson et al., 2016).
481 The MSGL orientation towards 083°E in area 1 differs significantly from the southeastward
482 drumlin orientation mapped across this area by the GSI (2016). Although topographic highs in the
483 area are mapped as drumlins, we see no indication of subglacial streamlining in a SE direction.
484 Neither is there evidence for ice flow northeastward, as proposed by Warren and others (Warren,
485 1992; Warren and Ashley, 1994; Pellicer et al., 2012). The evidence in area 1 points to active ice flow
486 eastward, toward an ice limit located beyond the study area.
487 *Stage 2:* MSGLs in area 1 are overlain by a geometric network of ridges and are interpreted
488 as crevasse-squeeze ridge (CSR) networks, formed during ice stagnation following accelerated ice
489 flow (Fig. 16). The ridges form by squeezing of highly deformable (wet) subglacial sediments into

490 extensional crevasses formed during accelerated ice flow (Sharp, 1985; Evans and Rea, 1999, 2003;
491 Evans et al., 2007; Rea and Evans, 2011).
492
493 Crevasse-squeeze ridges were first observed in association with surging glaciers, where
494 acceleration is relatively shortlived (tens of years or less) and often involve a readvance of the ice
495 margin (e.g., Meier and Post, 1969; Kamb et al., 1985; Ingólfsson et al., 2016). More recently, CSRs
496 have been observed in the footprint of palaeo ice streams (Ó Cofaigh et al., 2010; Evans et al., 2016),
497 where acceleration is more prolonged, and transition to a slower velocity regime occurs over 100s of
498 years (Catania et al., 2012; Evans et al. 2016). The expected ridge network geometry differs
499 between the two situations. TheCSRs formed by surging tend to occur as nets extending laterally
500 transverse to ice flow with a significant arcuate component to the overall ridge network (e.g., Evans
501 and Rea, 1999, 2003; Evans et al., 2016). The CSRs formed under ice streams are thought to form
502 confined corridors along the central part of the ice stream, where tensional crevasses are best
503 developed; ice stream CSRs are also likely to have well-developed transverse ridges reflecting this
504 (Evans et al., 2016).
505 The CSR network in area 1 is arranged in a relatively narrow corridor that continues to the
506 east of the LiDAR DTM, parallel to ice flow direction, but not to the north or south. The MSGLs also
507 extend eastward, and GSI (2016) and earlier mapping indicated further subglacial lineations and
508 esker fragments aligned parallel to these MSGLs up to 50 km east of area 1. This geometry is
509 consistent with formation along the trunk of a laterally confined glacier or ice stream and resembles
510 MSGL and rectilinear networks identified as the footprint of long-periodicity surging glaciers and
511 surging ice streams elsewhere (Andreasson et al., 2014; Evans et al., 2016; Flink et al., 2017).
512 *Stage 3:* CSR formation was followed by a period of relative ice mass stasis, down- and
513 backwasting accompanied by widespread glaciofluvial meltwater production and the consequent
514 formation of eskers and kames to the northwest and south of the MSGLs and CSRs (Fig. 16). These
515 features have been documented elsewhere and consist of subglacial conduit fills terminating in, or

516 overlain by, ice-marginal subaqueous sediments (Farrington with Synge, 1970; Warren and Ashley,
517 1994; Pellicer et al., 2012). The establishment of subglacial conduits under the ice sheet is
518 consistent with a switch from a high-pressure, distributed subglacial meltwater system to a relatively
519 low-pressure channelized system on the cessation of accelerated flow (Fig. 16; Kamb et al., 1985;
520 Raymond, 1987) and probably happened during, or shortly after, CSR formation, with esker
521 formation occurring towards the end of conduit life. Esker orientation indicates that these conduits
522 drained eastward.

523 Subsequently, ice recession westward and downslope resulted in the ponding of water along
524 the ice margin (Paleolake Riada), with the deposition of subaqueous outwash sediments at conduit
525 mouths (Fig. 16). These are represented by the Ballyduff esker and Blackwood kame-delta (Fig. 1;
526 Warren and Ashley, 1994; Pellicer et al., 2012) and indicate ice-marginal water flow was
527 northeastward. We consider this difference in esker orientation and ice-marginal water flow
528 direction to reflect a change from subglacial water flow driven by ice surface slope to ice-marginal
529 flow responding to a combination of ice margin geometry and local topography. This combination of
530 ice and water flow directions supports the interpretation of the Ballyduff esker as an interlobate
531 moraine (Warren and Ashley, 1994) but indicates that the dispersal centre for ice feeding the
532 southern lobe lies to the west of the Irish Midlands basin rather than the southwest.

533 During later westward ice-marginal recession, ENE-ward-trending conduit fills formed at the
534 southern margin of area 2. Their alignment supports models of ice flow deflection from
535 eastsoutheastward to eastnortheastward around the margin of the Slieve Bloom uplands (Fig. 16;
536 Gallagher et al., 1996).

537 *Stage 4:* Formation of MSGLs in areas 2 and 3 around Birr indicates a second phase of
538 accelerated, extensional ice flow, toward 127° (southeastward) (Fig. 16). This supports existing
539 interpretations of NW to SE ice flow in this area (Greenwood et al., 2009a,b). This flow direction is
540 at a high angle to preexisting eskers in the area and indicates ice marginal readvance during MSGL

541 formation, a possibility supported by the orientation of esker ridges formed during subsequent ice
542 sheet drainage (stage 5 below).
543 *Stage 5:* As in area 1, accelerated ice flow is followed by deceleration and ice stagnation,
544 resulting in the formation of CSRs (Fig. 16). The CSR formation in areas 2 and 3 involved significant
545 reworking of underlying MSGLs, so much so that in places only MSGL grooves remain. The overall
546 geometry of the CSR network also differs: CSRs occur as a ca.2-km-wide zone extending
547 southwestward across areas 2 and 3, interrupted only by major esker ridges occupying lower
548 ground. This geometry is consistent with formation of CSRs by surging of an ice marginal zone rather
549 than in a discrete corridor underlying a linear ice stream (Evans et al., 2016).
550 Ice stagnation following surging around areas 2 and 3 also involved a switch from a
551 distributed drainage system to drainage through intricate subglacial conduits, represented by the
552 interweaved formation of esker segments and subglacial meltwater channels (Fig. 16). This
553 subglacial drainage network was more complex than that formed in area 1, with closely spaced
554 larger conduits flanked by networks of subglacial Nye channels (in HT2) and by crevasse fills (in HT3)
555 indicating en- and supra-glacial diversion of water from conduits laterally across the sole of, and
556 upward into, the ice sheet. Clustering of these meltwater channels and conduits indicates high
557 meltwater discharges passing rapidly through the system and exceeding the carrying capacity of the
558 preexisting conduit system. The formation of these features points to the occurrence of a subglacial
559 outburst flood type event following CSR formation. The southeastward draining conduits also cross
560 older ENE-trending glaciofluvial ridges, indicating that they formed under a reorganised ice sheet
561 geometry that may reflect a shift in ice surface slope, consistent with an ice-margin readvance
562 model.
563 The combination of landforms in area 2 is characteristic of surging glacier landsystems
564 described in front of modern, temperate surging glaciers (e.g., Evans and Rea, 1999, 2003). The
565 occurrence of a readvance during surging, followed by a post-surge outburst flood is also a common
566 feature of modern surging glaciers (e.g., Kamb et al., 1985; Bennett et al., 2000; Eisen et al., 2005;

567 Burke et al., 2010). This surge event in the western part of the Irish Midlands basin post-dated the
568 accelerated flow associated with MSGL formation in the eastern part of the basin (at Area 1),
569 indicating that at least two distinct phases of accelerated flow occurred during overall deglaciation
570 of the region.
571
572 *Implications for dynamics of the Irish Ice Sheet:* Accelerated ice flow has previously been
573 associated with formation of extensive drumlin fields in the northern half of Ireland (Fig. 1) and with
574 formation of MSGLs in the Irish Sea basin associated with the Irish Sea ice stream (Van Langehem et
575 al., 2009). One theory is that the drumlins formed as a result of repeated surging initiated by
576 drawdown of ice in response to the rapid breakup of the Irish Sea Ice Stream by calving along the
577 tidewater margin of an 'Irish Sea Ice Stream' (Eyles and McCabe, 1989; McCabe, 1996; McCabe et al.,
578 1998). However, this model relies on an external trigger, i.e., episodic relative sea-level rise to
579 destabilise ice margins and to generate drumlin formation. It does not account for those drumlins
580 formed behind land-terminating ice margins of the last British Irish Ice Sheet. An alternative cause
581 of surging in these cases may be a disequilbrium within the ice sheet. Sevestre and Benn (2015)
582 showed that surging in modern glaciers is caused by imbalances in mass and enthalpy (defined as
583 the internal energy of glacier system) transfers within the glacier. We suggest that surging in the
584 Irish Midlands reflects a similar internal imbalance in the Irish Ice Sheet during deglaciation rather
585 than oscillations driven by external triggers such as relative sea-level influencing marine-terminating
586 ice sheet sectors.
587
588 Recent work on the morphometrics of drumlins and MSGLs suggests that they form a
589 continuum, with elongation controlled by a combination of glacier bed sedimentary properties, ice
590 velocity, and time (Barchyn et al., 2016, Jamieson et al., 2016). Greenwood and Clark (2008, 2010)
591 showed that drumlin length increases in a down-ice direction across the Irish Midlands, with MSGLs
592 occurring at the downstream end of some flow sets, and showed that this increase in length does

not reflect changes in the subglacial bed. Instead, they suggested that changes in velocity are the primary control on lineation length. The evidence for a temporal variation from ice streaming to a surging ice margin presented here suggests that the length of time over which accelerated flow phases operated may also have been a factor in controlling bedform lineation length. The reduction in lineation length westward across central Ireland therefore may reflect a reduction in ice flow velocity *and* length of time of accelerated flow.

Andreasson et al. (2014) suggested a similar transition in ice dynamics during recession around Svalbard. Surging glaciers with current cycle lengths in the region of 50-500 years (Sevestre and Benn, 2015) are linked offshore and through time to the location of former ice streams. Similar subglacial bedform assemblages to those occurring in central Ireland are preserved downstream from the modern termini of these glaciers (Otteson et al., 2007; Andreasson et al., 2014). Surging behaviour has also been observed in the Kamb ice stream, Antarctica, during overall ice retreat (Engelhardt and Kamb, 2013).

An external control on ice marginal dynamics during recession may have been the presence of a large proglacial lake (Paleolake Riada), as modern and Quaternary proglacial lakes have been linked to enhanced ice flow velocity, changing flow direction and enhancing retreat rates through iceberg calving (e.g., Kirkbride and Warren, 1999; Stokes and Clark, 2003; Walder et al., 2006; Tsutaki et al., 2013). The proglacial lake had not yet formed during MSGL and CSR formation in area 1, as the ice margin extended across the watershed. However, in area 2, the depth of Paleolake Riada was around 40 m at the ice margin during ice recession, possibly sufficient to have influenced ice flow velocity and direction during a local readvance. This may help explain the shift in ice surface slope direction and associated conduit orientation following surging.

The other impact of Paleolake Riada on the glacial landform assemblages seen in the LiDAR DTMs may have been to allow their preservation in the decades after ice sheet recession as subaqueous landforms, preventing proglacial fluvial and periglacial weathering and erosion. The removal of landforms along river floodplains is noticeable in areas 1 and 2, indicating Holocene

fluvial erosion. A further factor in landform preservation may be the widespread practice of pastoral farming in the Irish Midlands throughout the twentieth century, so that mechanised ploughing has not occurred over much of the area.

6. Conclusions

- Low-amplitude landforms revealed by high-resolution DTMs constructed from LiDAR provide evidence for two distinct phases of accelerated ice flow and subsequent stagnation in the central Irish Midlands. The first phase was associated with the operation of an eastward-directed ice stream extending beyond the bounds of the study area. Landforms associated with the second phase are typical of modern surging glacier landsystems
- Ice flow directions during both accelerated ice flow events are parallel to post-surge subglacial conduit orientations as indicated by nearby major eskers. These indicate that a switch occurred from a distributed basal meltwater drainage system to a more efficient channelized system at the cessation of accelerated flow. In addition, following the second surge event, a subglacial outburst flood formed tunnel channels that linked to ice-walled conduits down-ice. Discharge was sufficiently high to overwhelm the existing conduit system and expand laterally into crevasses.
- The high-resolution DTMs provide the first clear evidence for ice flow directions around the Tullamore area (area 1). This previously undetected subglacial lineation flowset indicates that ice flow in this area was eastward, during a phase of ice streaming during regional deglaciation.
- Overall, our work demonstrates the potential for airborne LiDAR surveys to enhance existing glacial geomorphological maps and to improve reconstructions of complex ice dynamics, even in areas previously mapped by remote sensing and fieldwork.

Acknowledgements

We thank the Office of Public Works, Ireland, for provision of LiDAR data for areas 1 and 3. LiDAR for area 2 was purchased at a reduced rate from Fugro-BKS Ltd. Purchase of LiDAR data covering area 2 was funded by Manchester Metropolitan University. We are grateful to an anonymous reviewer and Dr. Ian S. Evans for helpful reviews that have considerably improved this paper.

653 **References**

654 Andreasson, K., Winsborrow, M.C.M., Bjarnadóttir, L.R., Rüther, D.C., 2014. Ice stream
655 retreat dynamics inferred from an assemblage of landforms in the northern Barents Sea. Quaternary
656 Science Reviews 92, 246-257.
657
658 Barchyn, T.E., Dowling, T.P.F., Stokes, C.R., Hugenholtz, C.H., 2016. Subglacial bedform
659 morphology controlled by ice speed and sediment thickness. Geophysical Research Letters 439140,
660 7572-7580.
661 Benn, D.I., Evans, D.J.A., 2012. Glaciers and Glaciation. 2nd Edition. Hodder, London, 816pp.
662
663 Bennett, M.R., Huddart, D., Waller, R.I., 2000. Glaciofluvial crevasse and conduit fills as
664 indicators of supraglacial dewatering during a surge, Skeidararjökull, Iceland. Journal of Glaciology
665 46, 25-34.
666 Bjarnadóttir, L., Winsborrow, M.C.M., Andreassen, K., 2014. Deglaciation of the central
667 Barents Sea. Quaternary Science Reviews 92, 208-226.
668
669 Boulton, G.S., van der Meer, J.J.M., Hart, J.K., Beets, D., Ruegg, G.H.J., van der Wateren, F.M.,
670 Jarvis, J., 1996. Till and moraine emplacement in a deforming bed surge – an example from a marine
671 environment. Quaternary Science Reviews 15, 961-988.
672
673 Boulton, G.S., Lunn, R.J., Vidstrand, P., Zatsepin, S., 2007. Subglacial drainage by
674 groundwater-channel coupling, and the origin of esker systems: part 1 – glaciological observations.
675 Quaternary Science Reviews 26(7-8), 1067-1090.
676

677 Brennand, T.A, 1994. Macroforms, large bedforms and rhythmic sedimentary sequences in
678 subglacial eskers, south-central Ontario: implications for esker genesis and meltwater regime.
679 Sedimentary Geology 91, 9-55.
680
681 Brennand, T.A., 2000. Deglacial meltwater drainage and glaciodynamics: inferences from
682 Laurentide eskers, Canada. Geomorphology 32, 263-293.
683
684 Burke, M.J., Woodward, J., Russell, A.J., Fleisher, P.J., Bailey, P.K., 2010. The sedimentary
685 architecture of outburst flood eskers: a comparison of ground-penetrating radar data from Bering
686 Glacier, Alaska and Skeidarárjökull, Iceland. Geol. Soc. Am. Bull. 122, 1637-1645.
687
688 Catania, G., Hulbe, C., Conway, H., Scambos, T.A., Raymond, C.F., 2012. Variability in the
689 mass flux of the Ross ice streams, West Antarctica, over the last millennium. J. Glaciology 58(210),
690 741-752.
691
692 Clark, C.D., 1993. Mega-scale glacial lineations and cross-cutting ice-flow landforms. Earth
693 Surface Processes and Landforms 18(1), 1-29.
694
695 Clark, C.D., Meehan, R.T., 2001. Subglacial bedform geomorphology of the Irish Ice Sheet
696 reveals major configuration changes during growth and decay. J. Quaternary Science 16(5), 483-496.
697
698 Clark, C.D., Hughes, A.L.C., Greenwood, S.L., Jordan, C.J. and Sejrup, H.P., 2012. Pattern and
699 timing of retreat of the last British-Irish Ice Sheet. Quaternary Science Reviews 44, 112-146.
700
701 Cline, M.D., Iverson, N.R., Harding, C., 2015. Origin of washboard moraines of the Des
702 Moines Lobe: spatial analyses with LiDAR data. Geomorphology 246, 570-578.

Delaney C.A., 2001a. Esker formation and the nature of deglaciation: the Ballymahon esker, Central Ireland. North West Geography 1, 23–33.

Delaney C.A., 2001b. Morphology and sedimentology of the Rooskagh esker, Co. Roscommon. Irish Journal of Earth Sciences 19, 5-22.

Delaney C.A., 2002. Sedimentology of a glaciofluvial landsystem, Lough Ree area, Central Ireland: implications for ice margin characteristics during Devensian deglaciation. Sedimentary Geology 149, 111–126.

Delaney C.A., 2007. Seasonal controls on deposition of Late Devensian glaciolacustrine sediments, central Ireland. In: Hambrey, M.J., Christofferson, P., Glasser, N.P. and Hubbard, B. (Eds.), Glacial Sedimentary Processes and Products. Special Publication of the International Association of Sedimentologists 39, p. 149-163.

Dowling, T.P.F., Spagnolo, M., Möller, P., 2015. Morphometry and core type of streamlined bedforms in southern Sweden from high resolution LiDAR. Geomorphology 236, 54-63.

Eisen, O., Harrison,W.D., Raymond, C.F., Echelmeyer, K.A., Bender, G.A., Gorda, J.L.D., 2005. Variegated Glacier, Alaska, USA: a century of surges. Journal of Glaciology 51(174), 399-406.

Engelhardt, H., Kamb, B., 2013. Kamb Ice Stream flow history and surge potential. Annals of Glaciology 54630, 287-298.

728 Evans, D.J.A., 2009. Controlled moraines: origins, characteristics and palaeoglaciological
729 implications. Quaternary Science Reviews 28,183-208.
730
731 Evans, D.J.A., Hiemstra, J.F., 2005. Till deposition by glacier submarginal, incremental
732 thickening. Earth Surface Processes and Landforms 30(13), 1633-1662.
733
734 Evans, D.J.A., Rea , B.R., 1999. Geomorphology and sedimentology of surging glaciers: a
735 landsystems approach. Annals of Glaciology 28, 75-82.
736
737 Evans, D.J.A., Rea, B.R., 2003. Surging glacier landsystem. In: Evans, D.J.A. (Ed.), Glacial
738 Landsystems. Arnold, London, pp.259-288.
739
740 Evans, D.J.A., Twigg, D.R., Rea, B.R. & Shand, M., 2007. Surficial geology and geomorphology
741 of the Brúarjökull surging glacier landsystem. Journal of Maps 3(1), 349-367.
742
743 Evans, D.J.A., Clark, C.D., Rea, B.R., 2008. Landforms and sediment imprints of fast glacier
744 flow in the southwest Laurentide Ice Sheet. Journal of Quaternary Science 23, 249-272.
745
746 Evans, D.J.A., Strzelecki, M. Milledge, D.G., Orton, C., 2012. Hørbyebreen polythermal glacial
747 landsystem, Svalbard. Journal of Maps 8(2), 146-156.
748
749 Evans, D.J.A., Young, N.J.P. & Ó Cofaigh, C., 2014. Glacial geomorphology of terrestrial-
750 terminating fast flow lobes/ice stream margins in the southwest Laurentide Ice Sheet.
751 Geomorphology 204, 86-113.
752

753 Evans, D.J.A., Storrar, R.D., Rea, B.R., 2016. Crevasse-squeeze ridge corridors: diagnostic
754 features of late-stage palaeo-ice stream activity. Geomorphology 258, 40-50, DOI:
755 10.1016/j.geomorph.2016.01.017.
756
757 Eyles, N., Boyce, J.I., Barendregt, R.W., 1999. Hummocky moraine: sedimentary record of
758 stagnant Laurentide Ice Sheet lobes resting on soft beds. Sedimentary Geology 123, 163-174.
759
760 Eyles, N., McCabe, A.M., 1989. The Late Devensian (<22,000 BP) Irish Sea basin: The
761 sedimentary record of a collapsed ice sheet margin. Quaternary Science Reviews 8(4), 307-351.
762
763 Farrington, A., with Synge, F.M., 1970. The eskers of the Tullamore district. In: Stephens, N.,
764 Glasscock, R.E. (Eds.), Irish Geographical Studies in Honour of E. Estyn Evans. Queens University,
765 Belfast, p. 49-52.
766
767 Flink, A.E., Hill, P., Noormets, R., Kirchner, N., 2017. Holocene glacial evolution of Mohnbukta
768 in eastern Spitsbergen. Boreas, early view article, 24 August 2017, DOI:10.1111/bor.1227.
769
770 Gallagher, C., Thorp, M., Steenson, P., 1996. Glacier dynamics around Slieve Bloom, Central
771 Ireland. Irish Geography 29(2), 67-82.
772
773 Geological Survey of Ireland (GSI), 2016. Quaternary Sediments and Geomorphology. Open
774 Access dataset, March 2016. Available at: http://www.gsi.ie/Mapping.htm (last accessed July 2017).
775
776 Greenwood, S.L., Clark, C.D., 2008. Subglacial bedforms of the Irish Ice Sheet. Journal of
777 Maps 4(1), 332-357.
778

779 Greenwood, S.L., Clark, C..D., 2009a. Reconstructing the last Irish Ice Sheet 1: changing flow
780 geometries and ice flow dynamics deciphered from the glacial landform record. Quaternary Science
781 Reviews 28, 3085-3100.
782
783 Greenwood, S.L., Clark, C.D., 2009b. Reconstructing the last Irish Ice Sheet 2: a
784 geomorphologically-driven model of ice sheet growth, retreat and dynamics. Quaternary Science
785 Reviews 28, 3101-3123.
786
787 Greenwood, S., Clark, C.D., 2010. The sensitivity of subglacial bedform size and distribution
788 to substrate lithological control. Sedimentary Geology 232(3), 130-144.
789
790 Hughes, A.L.C., Gyllencreutz, R., Lohne, Ø.S., Mangerud, J., Svendsen, J.L., 2016. The last
791 Eurasian Ice Sheets – a chronological database and time-slice reconstruction, DATED-1. Boreas 45(1),
792 1-45.
793
794 Ingólfsson, Ó., Benediktsson, Í.Ö., Schomacker, A., Kjaer, K.H., Brynjólfsson, S., Jónsson, S.A,
795 Korsgaard, N.J., Johnson, M.D., 2016. Glacial geological studies of surge-type glaciers in Iceland –
796 research status and future challenges. Earth-Science Reviews 152, 37-69.
797
798 Jamieson, S.S.R., Stokes, C.R., Livingstone, S.J., Vieli, A., Ó Cofaigh, C., Hillenbrand, C.-D.,
799 Spagnolo, M., 2016. Subglacial processes on an Antarctic ice stream bed. 2: Can modelled ice
800 dynamics explain the morphology of mega-scale glacial lineations? Journal of Glaciology 62, 285-298.
801
802 Jónsson S.A., Schomacker A., Benediktsson Í.Ö., Ingólfsson Ó., Johnson M.D., 2014. The
803 drumlin field and the geomorphology of the Múlajökull surge-type glacier, central Iceland.
804 Geomorphology 207, 213–220.

Kamb, B., Raymond, C.F., Harrison, W.D., Engelhardt, H., Echelmeyer, K.A., Humphrey, N., Brugman, M.M., Pfeffer, T., l 1985. Glacier surge mechanism: 1982-1983 surge of Variegated Glacier, Alaska. Science 227(4684), 469-479.

Kirkbride, M.P., Warren, C.R., 1999. Tasman Glacier, New Zealand: 20th-century thinning and predicted calving retreat. Global & Planetary Change 22(1), 11-28.

Knight, J., McCarron, S.G., McCabe, A.M., 1999. Landform modification by palaeo-ice streams in east central Ireland. Annals of Glaciology 28, 195-207.

Kokalj, Ž., Zakšek, K., Oštir, K., 2011. Application of sky-view factor for the visulaization of historic landscape features in LiDAR-derived relief models. Antiquity 85 (327), 263-273.

Kruger, J., 1994. Glacial processes, sediments, landforms and stratigraphy in the terminus region of Myrdalsjökull, Iceland. Folia Geographica Danica 21, 233.

Mäkinen, J., Palmu, J.-P., 2008. Collapse of sediment-filled crevasses associated with floods and mass flows in the proximal zone of the Pernunnummi sandurdelta, III Salpausselkä, SW Finland. Quaternary Science Reviews 27, 1992-2011.

McCabe, A.M., 1996. Dating and rhythmicity from the last deglacial cycle in the British Isles. Journal of the Geological Society, London 153, 499-502.

McCabe, A.M., 2007. Glacial Geology and Geomorphology - The Landscapes of Ireland. Dunedin Academic Press, Edinburgh, 274p.

McCabe, A.M., Knight, J., McCarron, S.G., 1998. Evidence for Heinrich event 1 in the British Isles. Journal of Quaternary Science 13, 549-568.

Meehan, R.T., 1999. Directions of ice flow during the last glaciation in counties Meath, Westmeath and Cavan, Ireland. Irish Geography 32, 26-51.

Meier, M.F., Post, A., 1969. What are glacier surges? Canadian Journal of Earth Sciences 6,807-817.

Möller, P., Dowling, T.P.F., 2015. The importance of thermal boundary transitions on glacial geomorphology: mapping of ribbed/hummocky moraine and streamlined terrain from LiDAR, over Småland, South Sweden. GFF 37,252-283.

Ó Cofaigh, C., Evans, D.J.A., Smith, I.R., 2010. Large-scale reorganization and sedimentation of terrestrial ice streams during late Wisconsinan Laurentide Ice Sheet deglaciation. Bulletin of the Geological Society of America 122, 743-756.

Ó Cofaigh, C., Stokes, C.R., Lian, O.B., Clark, C.D., Tulacyzk., S., 2013. Formation of mega-scale glacial lineations on the Dubawnt Lake Ice Stream bed: 2. Sedimentology and stratigraphy. Quaternary Science Reviews, 77, 210-227.

Ottesen, D., Dowdeswell, J.A., Benn, D.I., Kristensen, L., Christiansen, H.H., Christensen, O. Hansen, L., Lebesbye, E., Forwick, M., Vorren, T.O., 2008. Submarine landforms characteristic of glacier surges in two Spitzbergen fjords. Quaternary Science Reviews 27, 1583-1599.

857 Pellicer, X.M., Warren, W.P., Gibson, P., Linares, R., 2012. Construction of an evolutionary
858 deglaciation model for the Irish midlands based on the integration of morphostratigraphic and
859 geophysical data analyses. Journal of Quaternary Science 27(8), 807-818.
860
861 Perkins, A.J., Brennand, T.A., Burke, M.J., 2016. Towards a morphogenetic classification of
862 eskers: Implications for modelling ice sheet hydrology. Quaternary Science Reviews 134, 19-38.
863
864 Price, R.J., 1970. Moraines at Fjallsjökull, Iceland. Arctic and Alpine Research 2(1), 27-42.
865
866 Raymond, C.F., 1987. How do glaciers surge? A review. Journal of Geophysical Research
867 92(B9), 9121-9134.
868
869 Rea, B.R., Evans, D.J.A., 2011. An assessment of surge-induced crevassing and the formation
870 of crevasse squeeze ridges. Journal of Geophysical Research: Earth Surface 116 (F4), F04005.
871
872 Roberts, M.J., Russell, A.J., Tweed, F.S., Knudsen, O., 2000. Ice fracturing during jökulhlaups:
873 implications for englacial floodwater routing and outlet development. Earth Surface Processes and
874 Landforms 25, 1429-1446.
875
876 Roering, J.J., Mackey, B.H., Marshall, J.A., Sweeney, K.E., Deligne, N.I., Booth, A.M.,
877 Handwerger, A.L, Cerovski-Darriau, C., 2013. 'You are HERE': connecting the dots with airborne
878 LiDAR for geomorphic fieldwork. Geomorphology 200, 172-183.
879
880 Russell, A.J., Roberts, M.J., Fay, H., Marren, P.M., Cassidy, N.J., Tweed, F.S., Harris, T., 2006.
881 Icelandic jökulhlaup impacts: Implications for ice-sheet hydrology, sediment transfer and
882 geomorphology. Geomorphology 75, 33-64.

883

884 Sevestre, H., Benn, D.I., 2015. Climatic and geometric controls on the global distribution of
885 surge-type glaciers: implications for a unifying model of surging. Journal of Glaciology 61(228), 646-
886 662.

887 Sevastopulo, G.D. and Wise-Jackson, P.N., 2009. Carboniferous: Mississippian (Tournaisian
888 and Viséan). In: Holland, C., Sanders, I. (Eds.), The Geology of Ireland. Dunedin Academic Press,
889 Edinburgh, 2nd edition, pp. 215-268.

890

891 Sharp, M.J., 1984. Annual moraine ridges at Skálafellsjökull, south-east Iceland. Journal of
892 Glaciology 50, 82-95.

893

894 Sharp, M., 1985. “Crevasse-fill” ridges – a landform type characteristic of surging glaciers?
895 Geografiska Annaler 67A, 213-220.

896

897 Slatton, K.C., Carter, W.E., Shrestha, R.L., Dietrich, W., 2007. Airborne laser swath mapping:
898 achieving the resolution and accuracy required for geosurficial research. Geophysical Research
899 Letters 34 (23), L23S10.

900

901 Smith, M.J., Rose, J., Booth, S., 2006. Geomorphological mapping of glacial landforms from
902 remotely sensed data: an evaluation of the principal data sources and an assessment of their quality.
903 Geomorphology 76, 148-165.

904

905 Sollas, W.J., 1896. A map to show the distribution of eskers in Ireland. Royal Dublin Society
906 Scientific Transactions 5(Series 2), 785-822.

907

908 Spagnolo, M., Clark, C.D., Ely, J.C., Stokes, C.R., Anderson, J.B., Andreassen, K., Graham,
909 A.G.C., King, E.C., 2014. Size, shape and spatial arrangement of mega-scale glacial lineations from a
910 large and diverse dataset. Earth Surface Processes and Landforms 39, 1432-1448.
911
912 Stokes, C.R., Clark, C.D., 2001. Palaeo-ice streams. Quaternary Science Reviews 20, 1437-
913 1457.
914
915 Stokes, C.R., Clark, C.D., 2003. The Dubawnt Lake palaeo-ice stream: evidence for dynamic
916 ice sheet behaviour on the Canadian shield and insights regarding the controls on ice stream location
917 and vigour. Boreas 32, 263-279.
918
919 Storrar, R.D., Stokes, C.R., Evans, D.J.A., 2014. Morphometry and pattern of a large sample
920 (>20,000) of Canadian eskers and implications for subglacial drainage beneath ice sheets.
921 Quaternary Science Reviews 105, 1-25.
922
923 Synge, F.M., 1952. Retreat stages of the last ice-sheet in the British Isles. Irish Geography
924 2(4), 168-171.
925
926 Synge, F.M., 1979. Quaternary glaciation in Ireland. Quaternary Newsletter 28, 1-18.
927
928 Synge, F.M., Stephens, N., 1960. The Quaternary Period in Ireland – an assessment. Irish
929 Geography 4, 121-130.
930
931 Tsutaki, S., Sugiyama, S., Nishimura, D., Funk, M., 2013. Acceleration and flotation of a glacier
932 terminus during formation of a proglacial lake in Rhonegletscher, Switzerland. J. Glaciolology 59,
933 559-570.

Walder, J.S., Trabant, D.C., Cunico, M., Fountain, A.G., Anderson, S.P., Anderson, R.S., Malm, A., 2006. Local response of a glacier to annual filling and draining of an ice-marginal lake. Journal of Glaciology 52(178), 440.

Warren, W.P., 1987. Site 5, Cappancur. In: Hammond, R.F., Warren, W.P., Daly, D. (Eds.), Offaly and West Kildare. Field Guide No. 10. Irish Association for Quaternary Studies, p. 43-45.

Warren, W.P., 1992. Drumlin orientation and the pattern of glaciation in Ireland. Sveriges Geologiska Undersökning Series CA 81, 359-366.

Warren WP, Ashley GM., 1994. Origins of the ice-contact stratified ridges (Eskers) of Ireland. Journal of Sedimentary Research A64, 433–449.

Zakšek, K., Oštir, K., Kokalj, Ž., 2011. Sky-view factor as a relief visualization technique. Remote Sensing 3, 398-415.

951 **FIGURE CAPTIONS**

952

953 Fig. 1.(A) Map of Ireland showing main glacial features and location of (B) (after Synge, 1979;
954 redrawn by P. Coxon). (B) Map of central Midlands basin showing position of LiDAR DTM, main
955 glacial landforms and places mentioned in the text. Land below 82 MOD is shaded grey-blue,
956 indicating areas likely to have been covered by Paleolake Riada when an ice dam was in place west
957 of the River Shannon and south of Birr. Eskers mapped by C. Delaney; drumlins and MSGLs mapped
958 by Geological Survey of Ireland (2016). TWO COLUMN WIDTH

959

960 Fig. 2. Published models of ice flow directions in the Irish Midlands. (A) Model of the Irish Ice
961 Sheet by Warren (1992) showing ice flowing northeast- and southeast-ward across the area
962 discussed in this paper, from ice domes to the north and southwest. Grey arrows added to the
963 original diagram show ice flow directions implied by dome contours. (B) Ice flowsets constructed
964 from subglacial lineations (drumlins and MSGLs) in the area around central Irish Midlands esker
965 system, from Greenwood et al. (2009a, b). Multiple flow directions can be inferred from subglacial
966 bedforms around the eskers. The area discussed in this paper is outlined. TWO COLUMN WIDTH

967

968 Fig. 3. (A) LiDAR DTM of Tullamore area, central Ireland. MSGLs and rectilinear grids of small
969 ridges are visible. Locations of Figs. 4 and 5 are shown. X – location of exposure in MSGL discussed in
970 text and shown in Fig. 6. Y – position of location illustrated in Fig. 7. (B) Interpretative sketch of
971 glacial features, including MSGL and crevasse-squeeze ridge (CSR) network fragments. (C) Cross
972 section of transverse ridge terrain at Cappancur, east of Tullamore town. TWO-COLUMN WIDTH

973

974 Fig. 4. (A) Closeup of hill-shaded DTM shown in Fig. 3A, showing the eastern part of rea 1
975 (location shown in Fig. 3A). The DTM shows MSGL crests and grooves and a partly preserved grid of
976 cross-cutting ridges, interpreted as crevasse-squeeze ridges (CSRs). Arrows indicate points where an

977 underlying ridge has been truncated by formation of the overlying ridge. MSGLs are visible towards
978 the bottom of the image. (B) PCA of hillshade shown in Fig. 4A. Arrows indicate points where ridges
979 have been truncated by the overlying ridge formation. (C) Interpretative sketch of glacial features
980 shown in Figs. 4A and 4B. ONE-COLUMN WIDTH
981
982 Fig. 5. (A) Closeup of southern part of hill-shaded DTM shown in Fig. 3A, showing part of an
983 esker, MSGL and the CSR network south of Tullamore town. (B) Interpretation sketch of glacial
984 features shown in Fig. 5A. ONE-COLUMN WIDTH
985
986 Fig. 6. (A) Exposure in MSGL showing highly compacted, silty diamicton. (B) Sheared clast
987 within diamicton. The location of the exposure is marked X in Fig. 3A. ONE-COLUMN WIDTH
988
989 Fig. 7. Photomontage of exposure at Y on Fig. 2A with interpretative sketch. TWO-COLUMN
990 WIDTH
991
992 Fig. 8. LiDAR DTM of area 2, Birr, showing glacial landforms and position of figures. MSGL,
993 hummocky terrain, and eskers are visible. Letters refer to landforms mentioned in the text. TWO-
994 COLUMN WIDTH
995
996 Fig. 9. Interpretation of landforms seen in area 2 DTMs and in surrounding area (mapped
997 using air photos). TWO COLUMN WIDTH
998
999 Fig. 10. (A) LiDAR DTM of area 3, southwest of area 2, showing type 1 hummocky terrain
1000 (HT1) and glaciofluvial ridges. (B) Interpretative sketch of landforms seen in (A). ONE-COLUMN
1001 WIDTH
1002

1003 Fig. 11. Closeup of MSGLs in area 2. Orientation is 307-127°. An esker is visible at the bottom
1004 left of the image. ONE-COLUMN WIDTH
1005
1006 Fig. 12. LiDAR DTM closeups and interpretations of hummocky terrain types. (A) and (B) HT1.
1007 (C) and (D) HT2. (E) and (F) HT3. TWO-COLUMN WIDTH
1008
1009 Fig. 13. Rose diagrams of ridge and groove orientations in hummocky terrain (HT). (A) HT1
1010 ridges. (B) HT1 grooves. (C) HT2 ridges. (D) HT2 grooves. (E) HT1 ridges in Area 3. (F) HT1 grooves in
1011 area 3.
1012
1013 Fig. 14. (A) Conduit fill sediments, esker B. (B) Beach deposits overlying conduit fill
1014 sediments in esker A. (C) Interbedded horizontal and cross-bedded pebble and cobble gravels,
1015 horizontally bedded and ripple laminated coarse to fine sands and ripple- and drape-laminated fine
1016 sands and silts, subaqueous outwash fan, esker A. (D) Climbing-ripple cross-laminated and drape-
1017 laminated fine sands and silts, esker F. TWO-COLUMN WIDTH
1018
1019 Fig. 15. (A) Short ridges extending of flat-topped ridge, interpreted as possible beach ridges
1020 reworked from esker sediments. (B) Overlapping eskers. Eskers X, Y, Z override esker A, formed at an
1021 earlier point in time. ONE COLUMN WIDTH
1022
1023 Fig. 16. Model showing successive stages in the deglaciation of the central Midlands.
1024 Individual stages are explained in the text.

Figure 1:

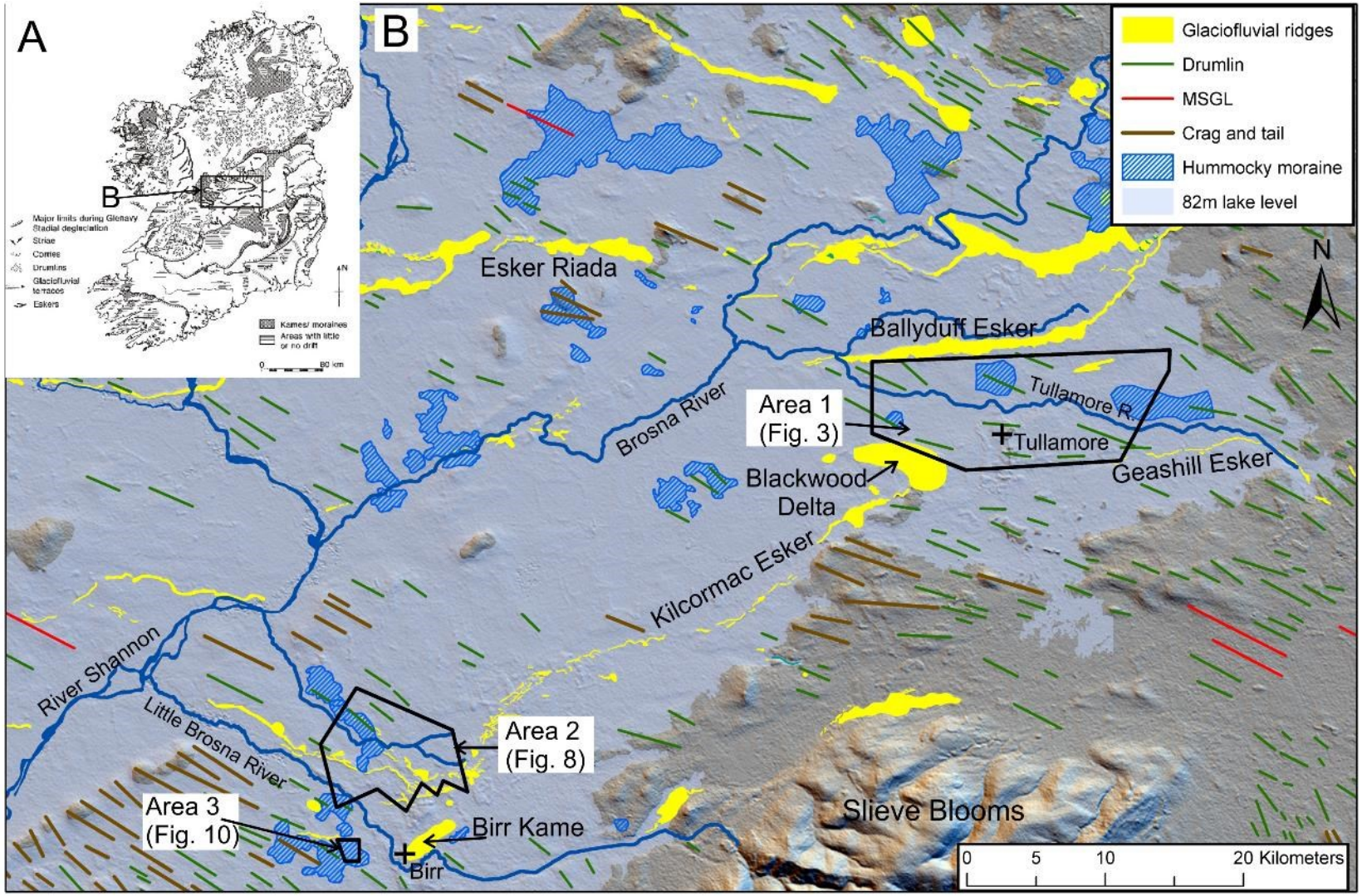
A
B
Major limits during Glenavy Stadial deglaciation
Striae
Corries
Drumlins
Glaciofluvial terraces
Eskers
Kames/ moraines
Areas with little or no drift
0
80 km
N
Glaciofluvial ridges
Drumlin
MSGL
Crag and tail
Hummocky moraine
82m lake level
Esker Riada
Ballyduff Esker
Tullamore R.
Area 1
(Fig. 3)
Tullamore
Brosna River
Geashill Esker
Blackwood
Delta
Kilcormac Esker
River Shannon
Little Brosna River
Area 2
(Fig. 8)
Area 3
(Fig. 10)
Birr Kame
Birr
Slieve Blooms
0
5
10
20 Kilometers

1027 Figure 2:

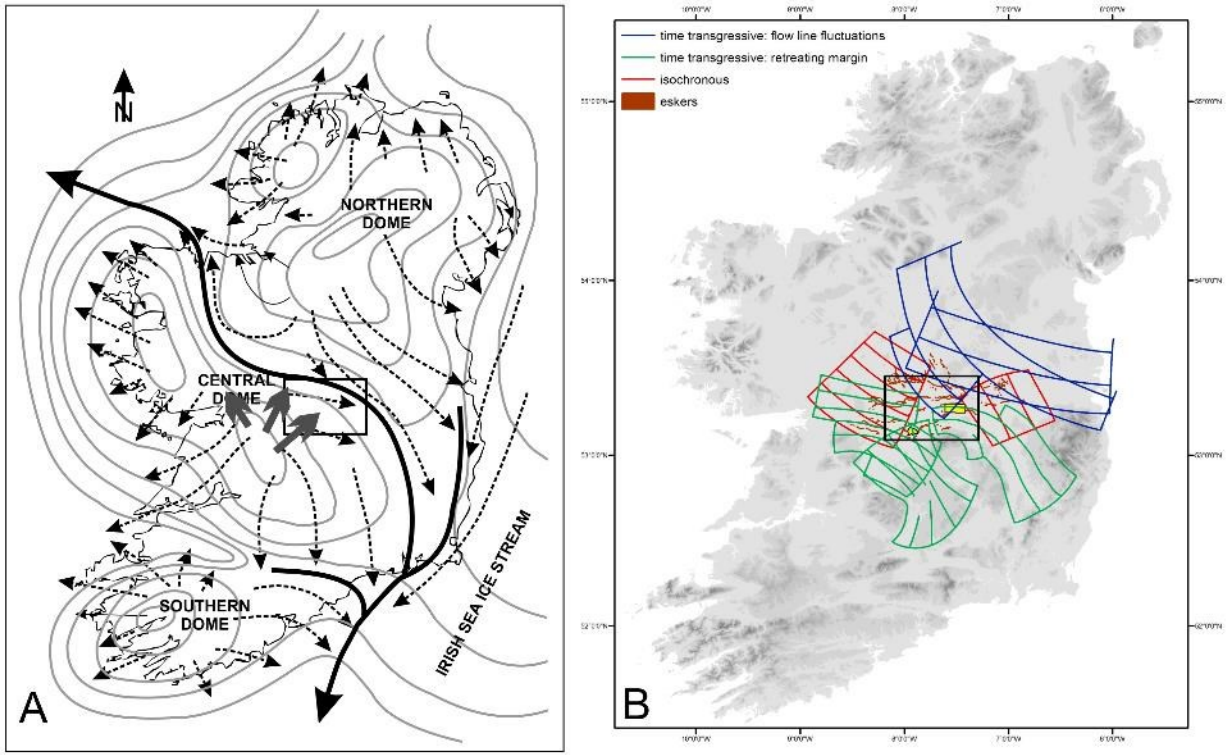

1028

1029 Figure 3:

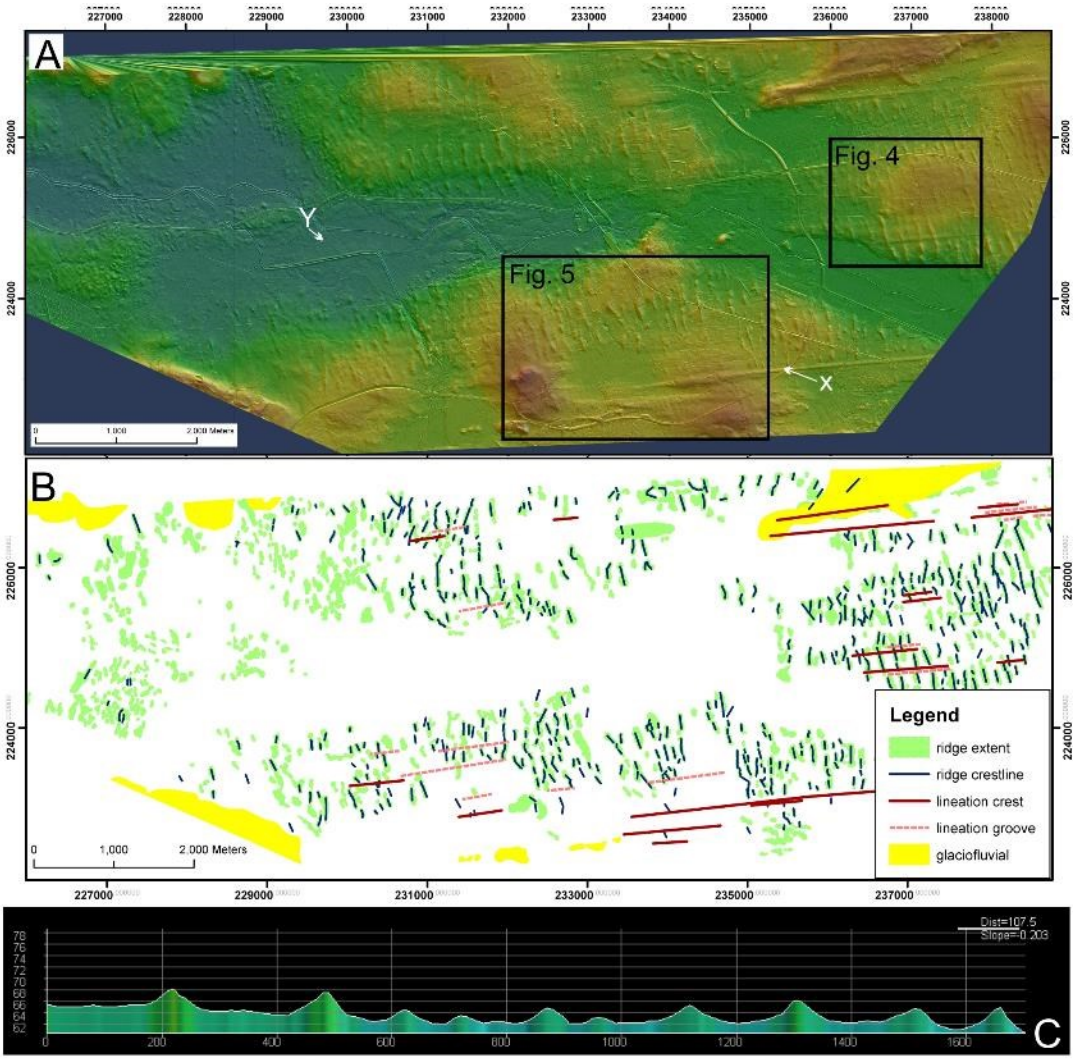

1030

1031 Figure 4:

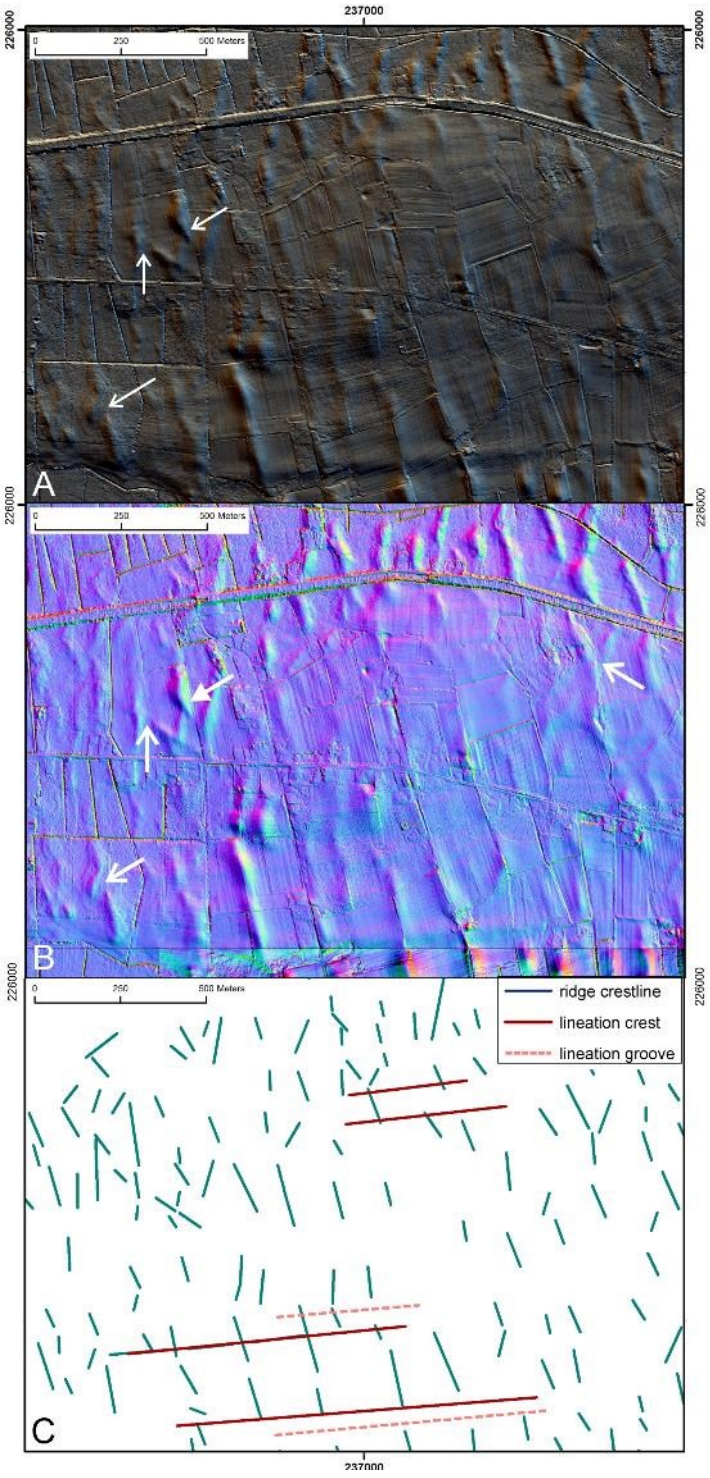

1032

1033 Figure 5:

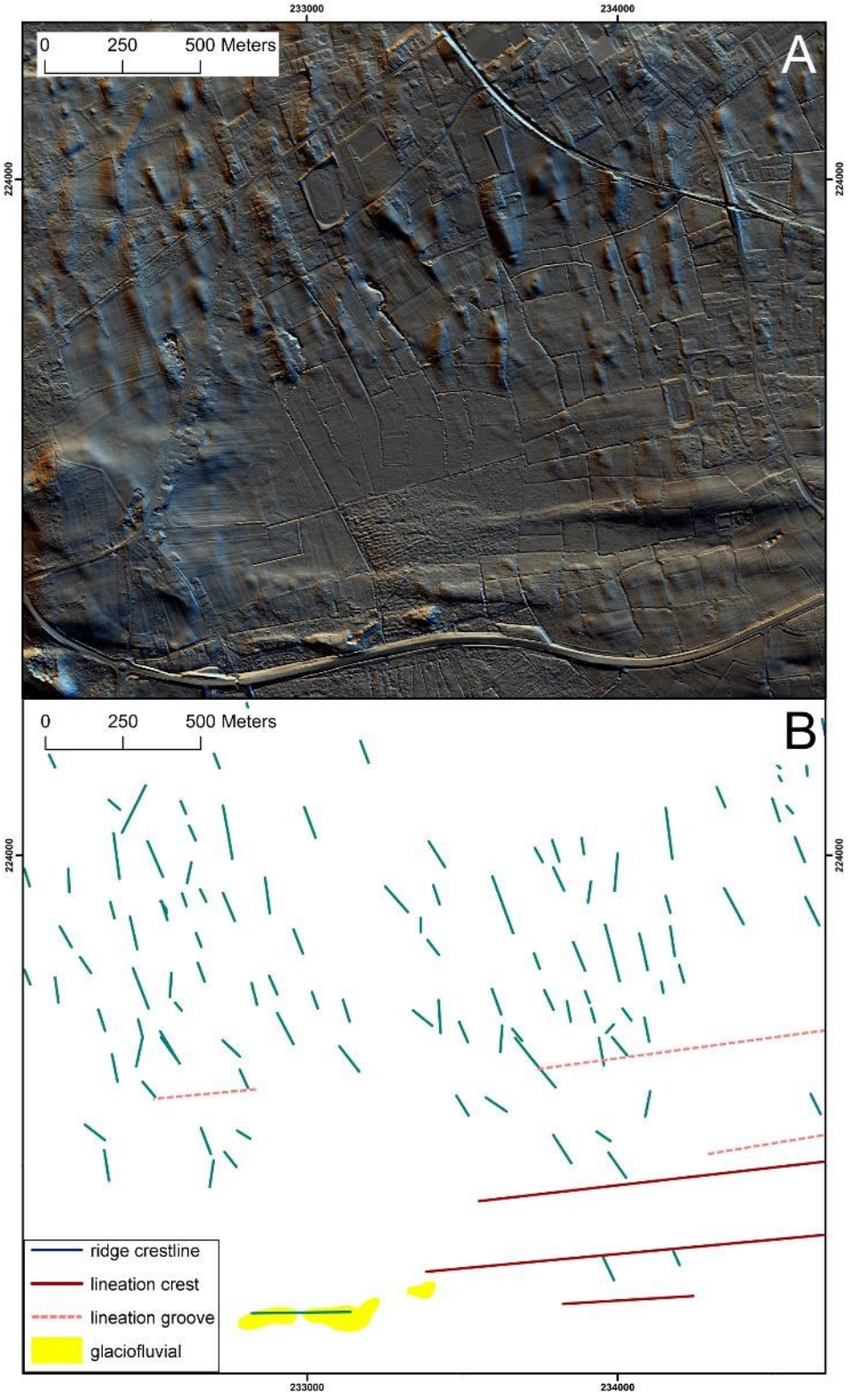

1034

1035 Figure 6:

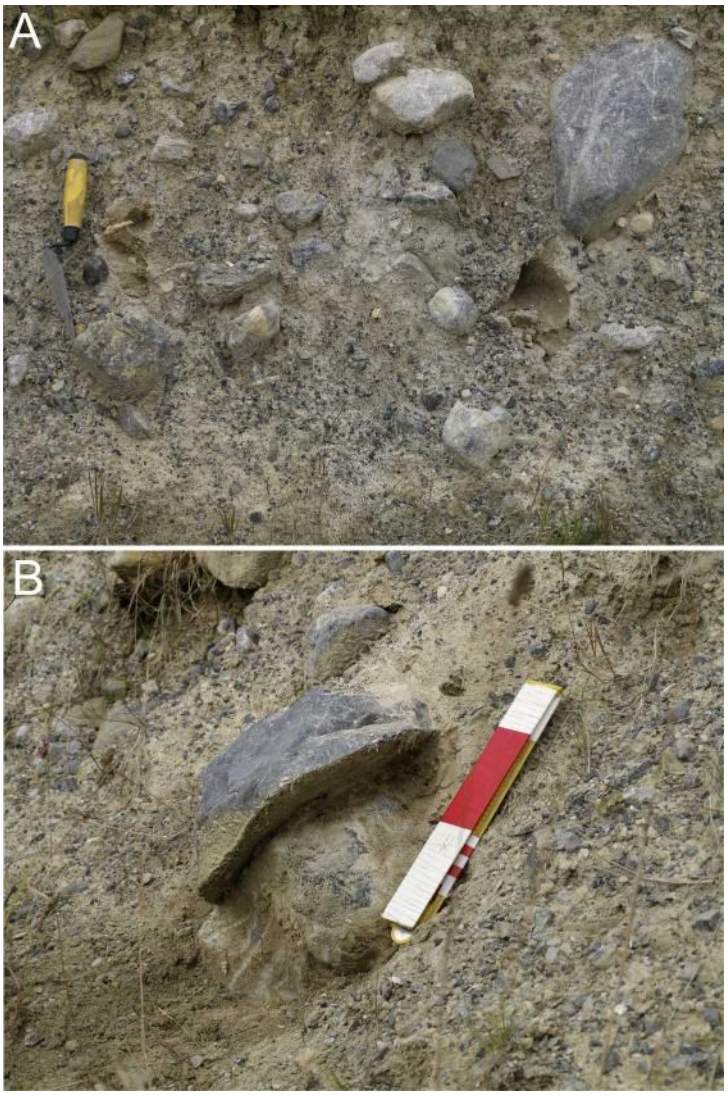

1036

1037 Figure 7:

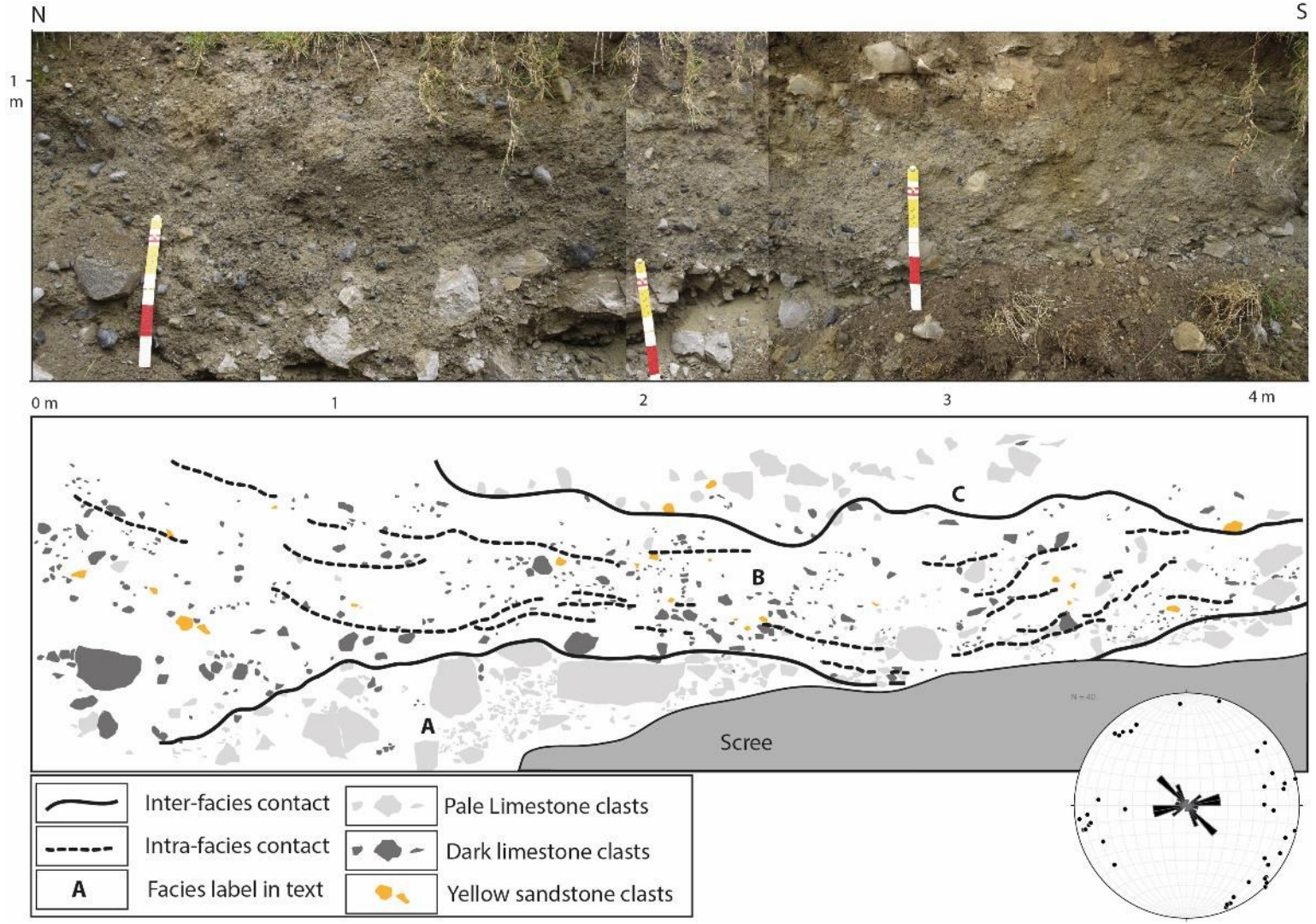

1038

1039 Figure 8:

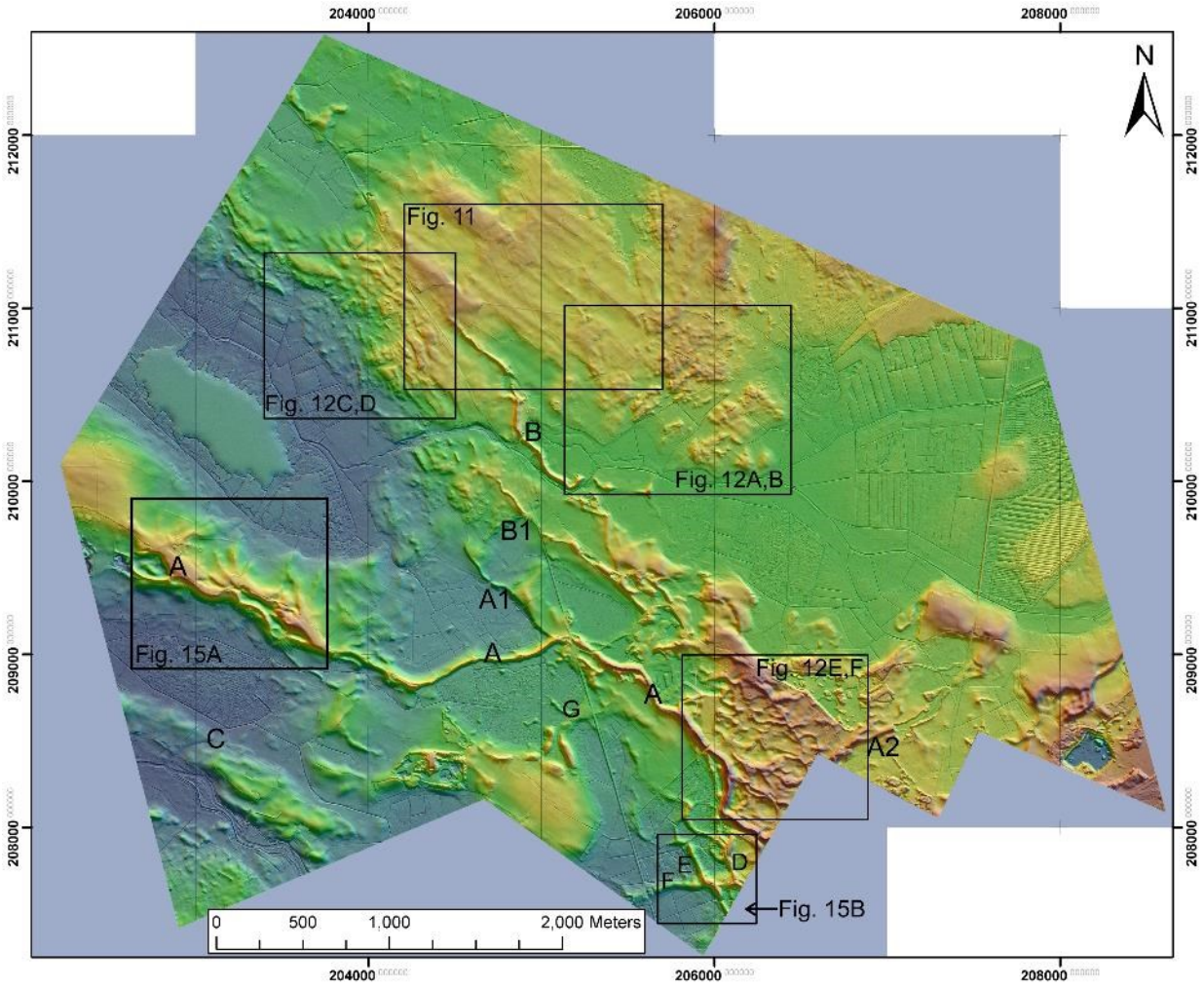

1040

Figure 9:

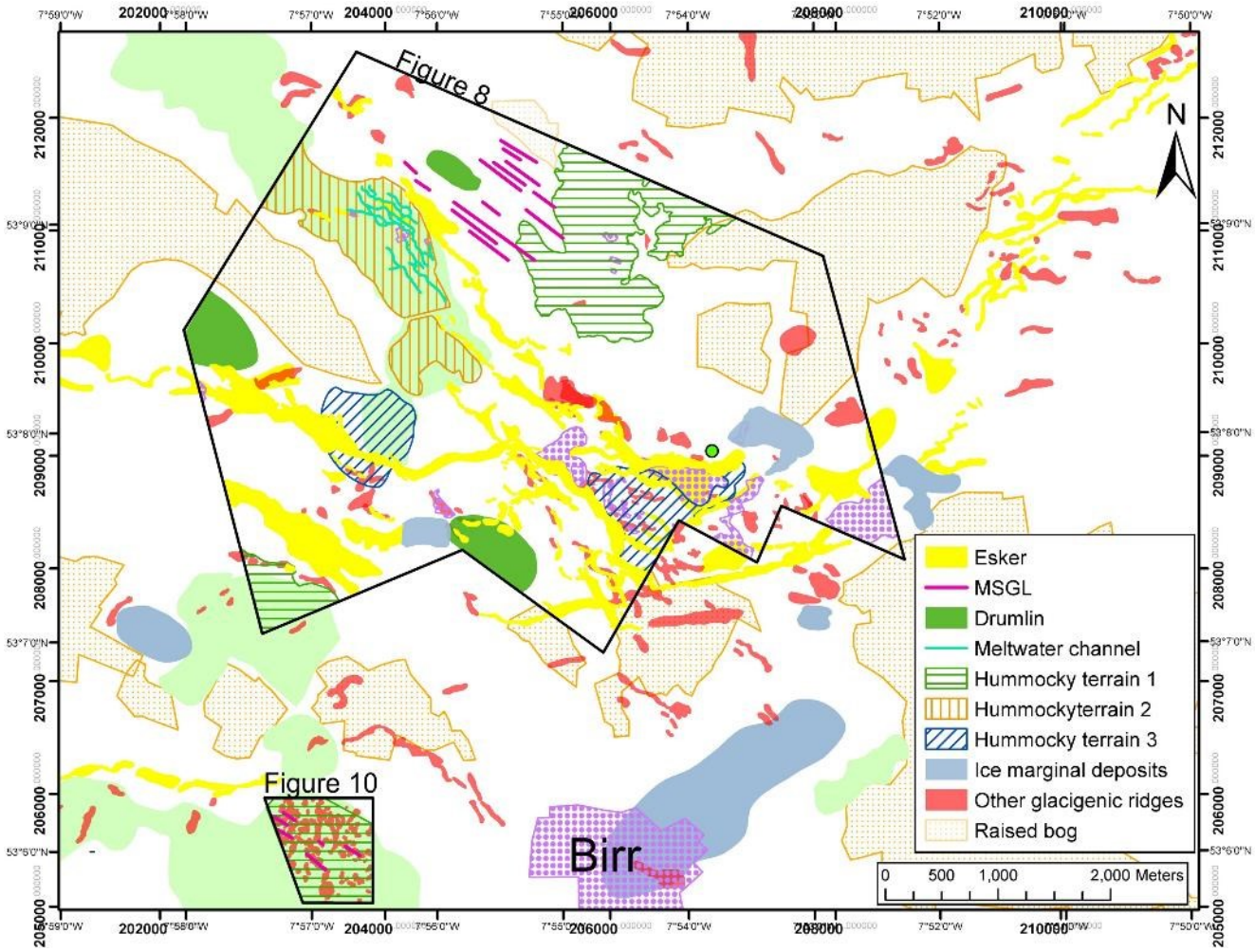
Figure 8
Figure 10
Birr
N
Esker
MSGL
Drumlin
Meltwater channel
Hummocky terrain 1
Hummockyterrain 2
Hummocky terrain 3
Ice marginal deposits
Other glacigenic ridges
Raised bog
0 500 1,000 2,000 Meters

1043 Figure 10:

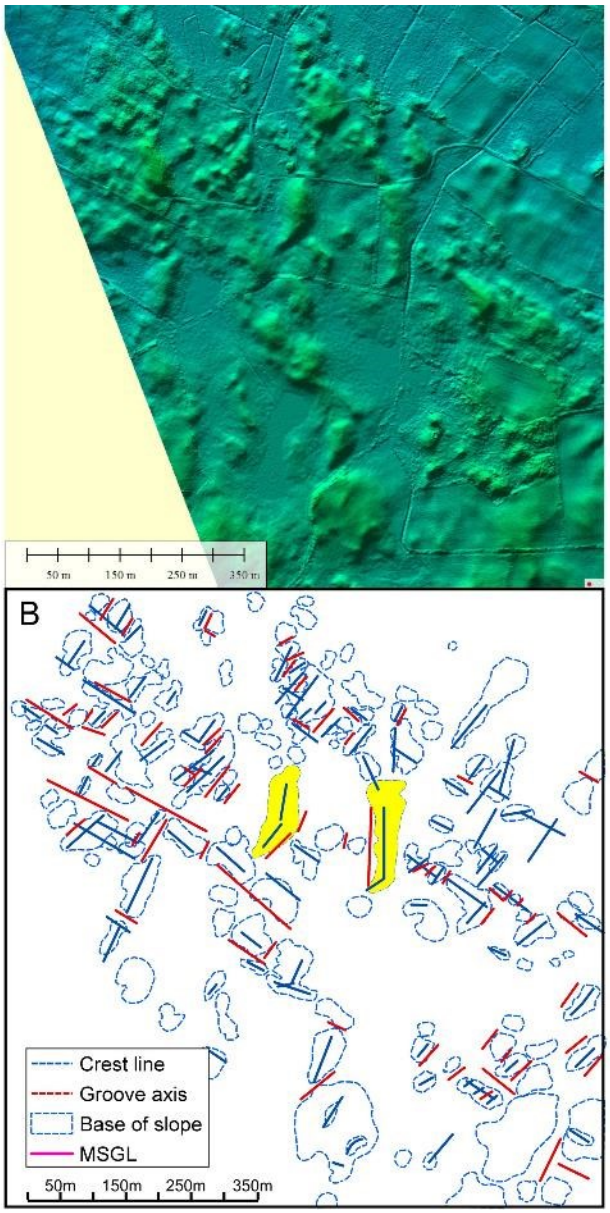

1044

1045 Figure 11:

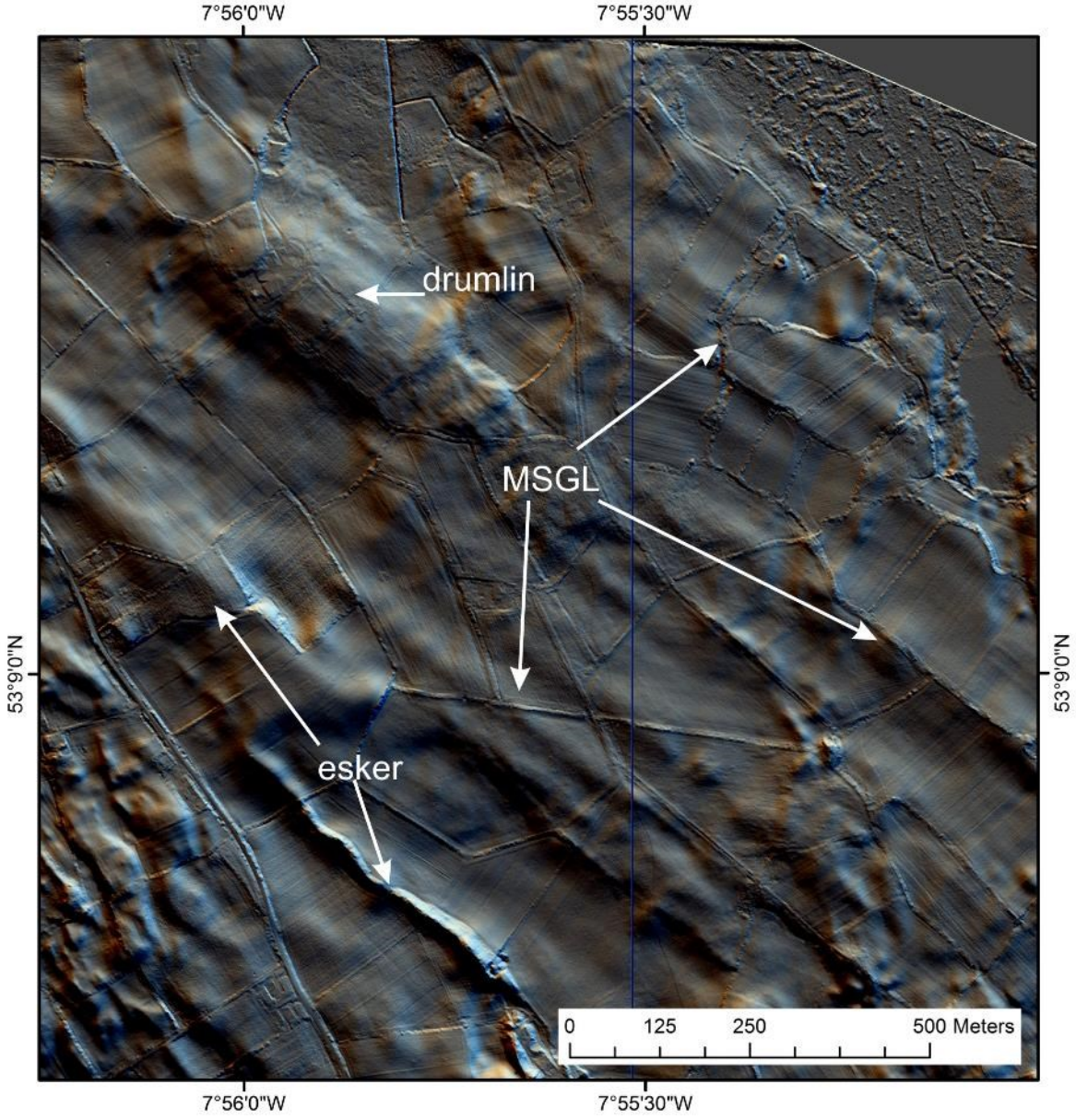

1046

1047 Figure 12:

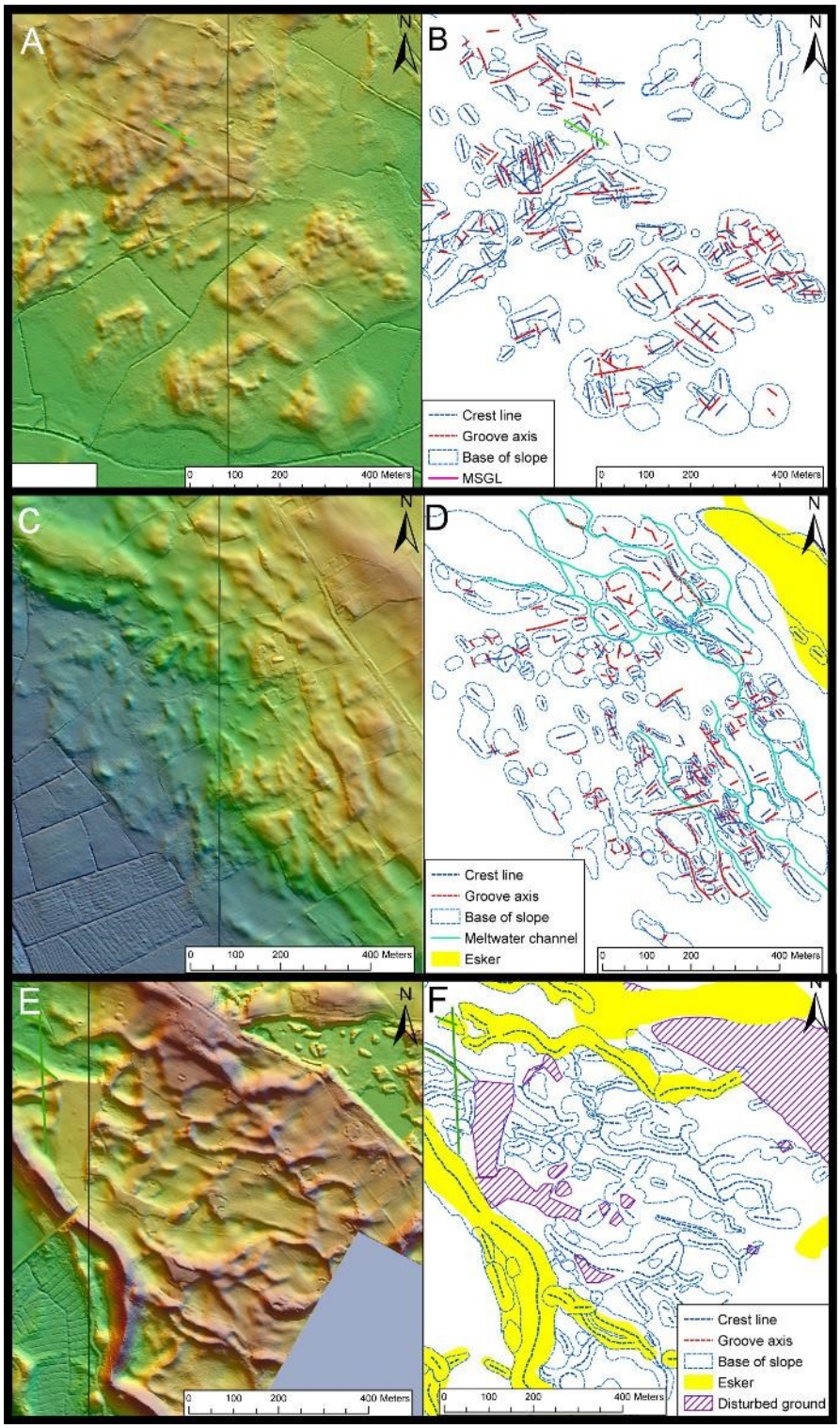

1048

1049 Figure 13:

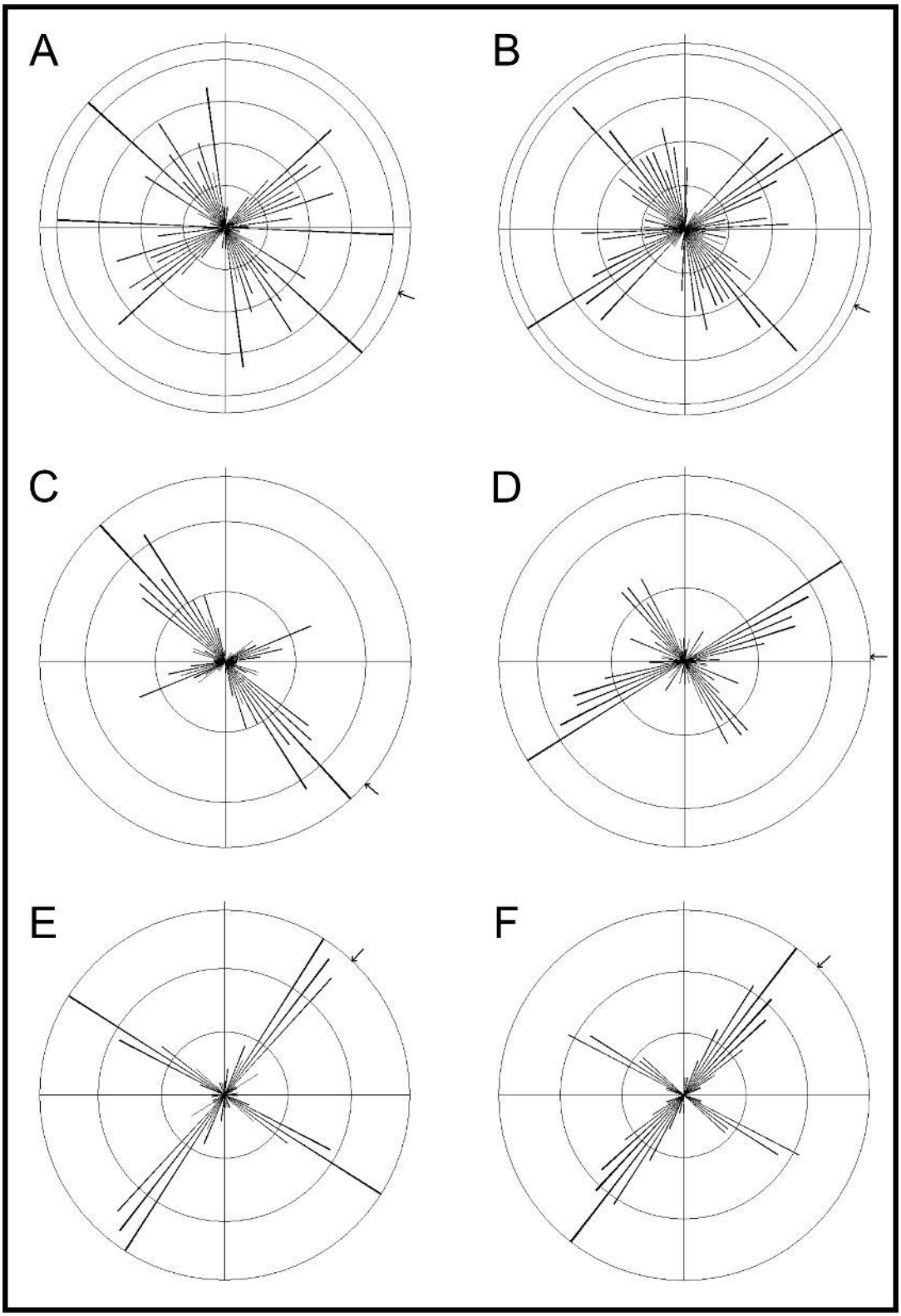

1050

1051 Figure 14:

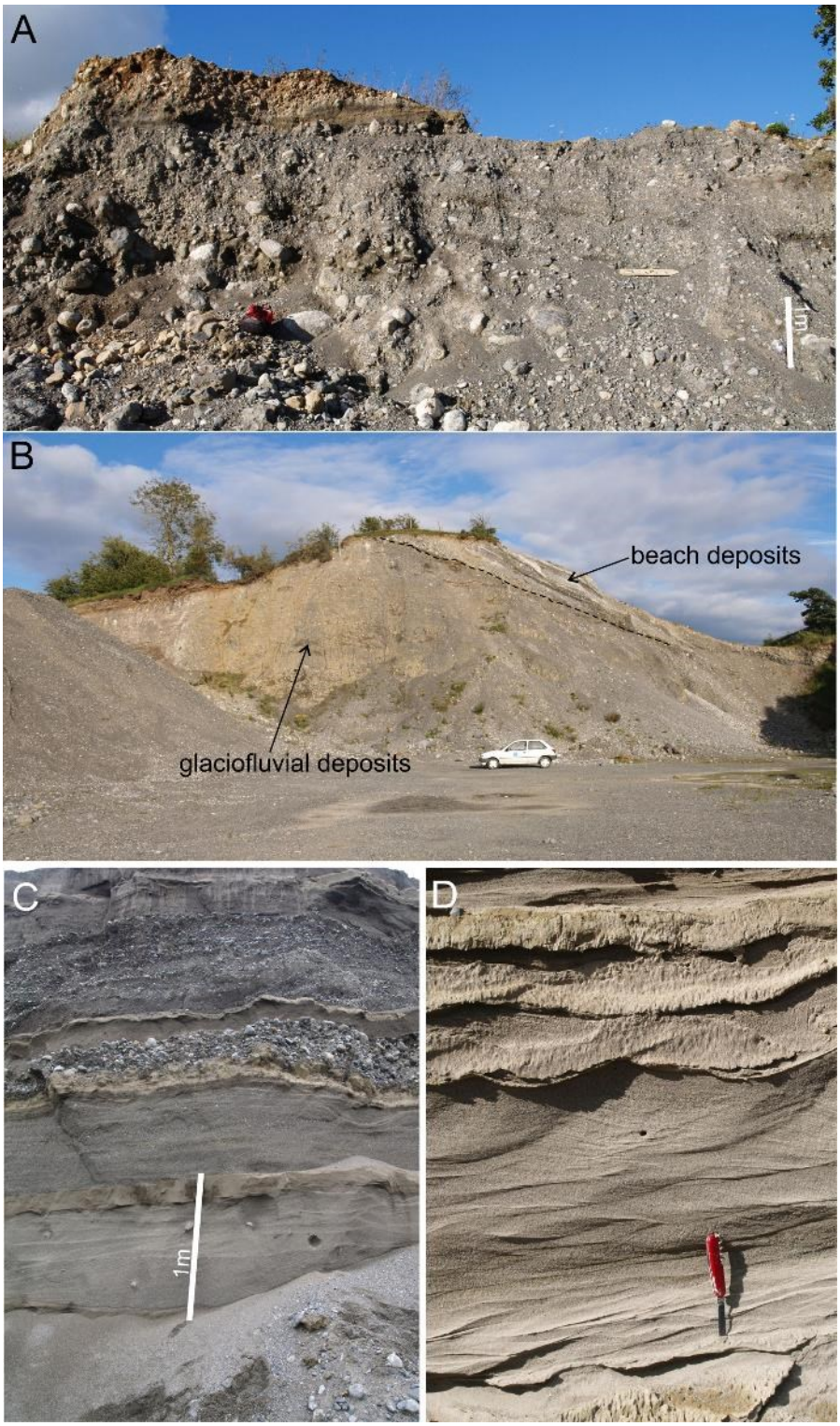

1052

1053 Figure 15:

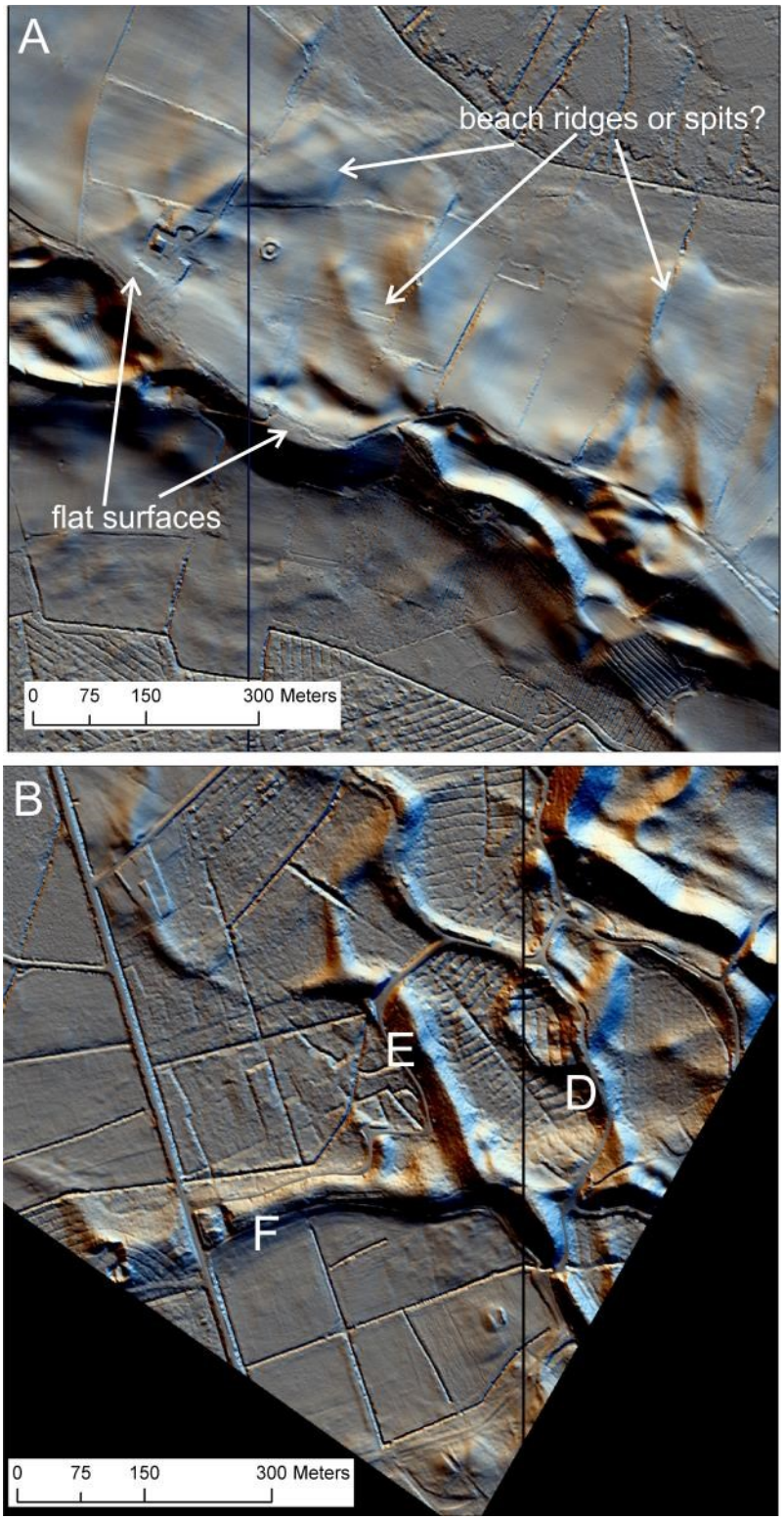

1054

1055 Figure 16:

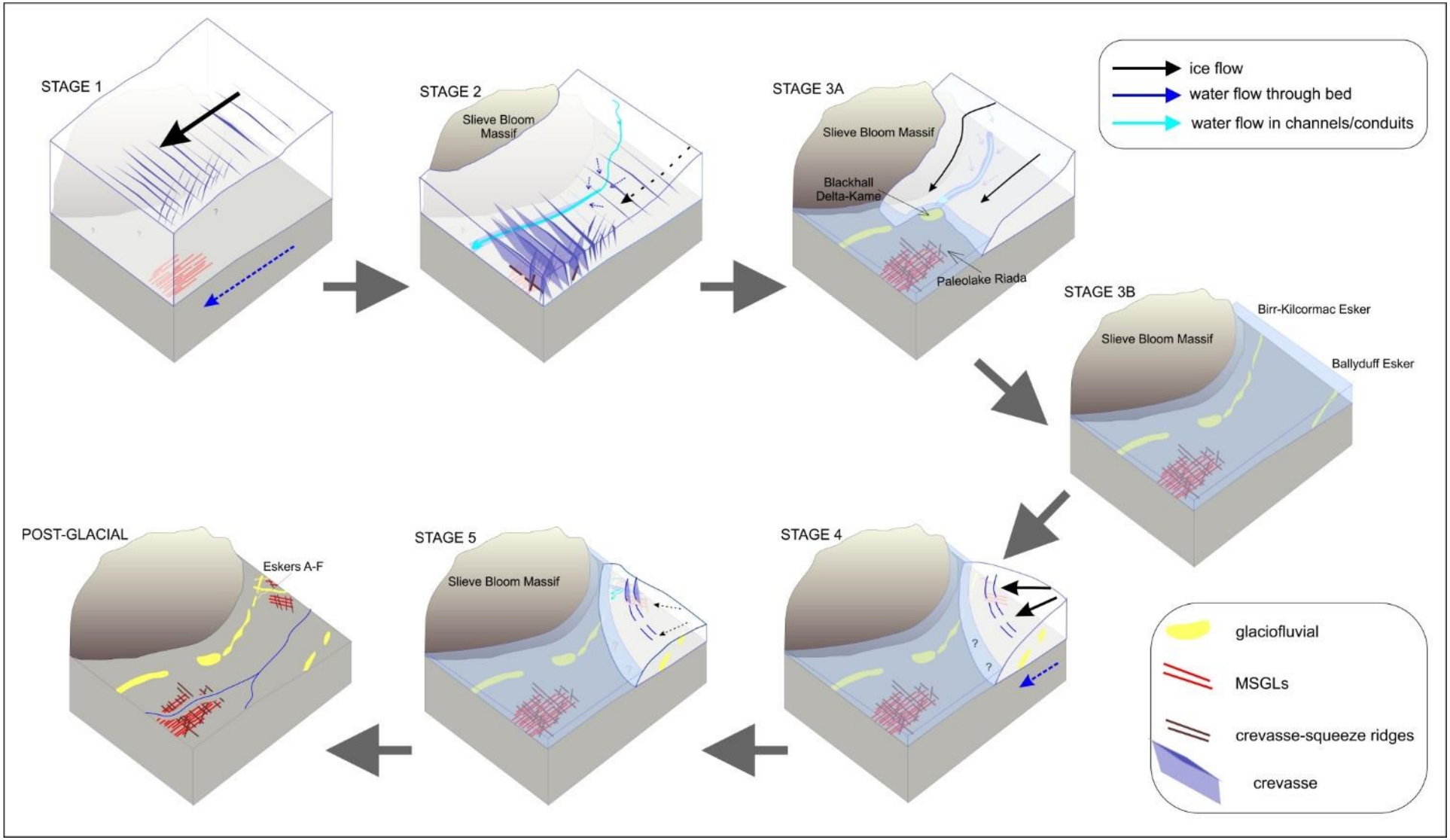

1056

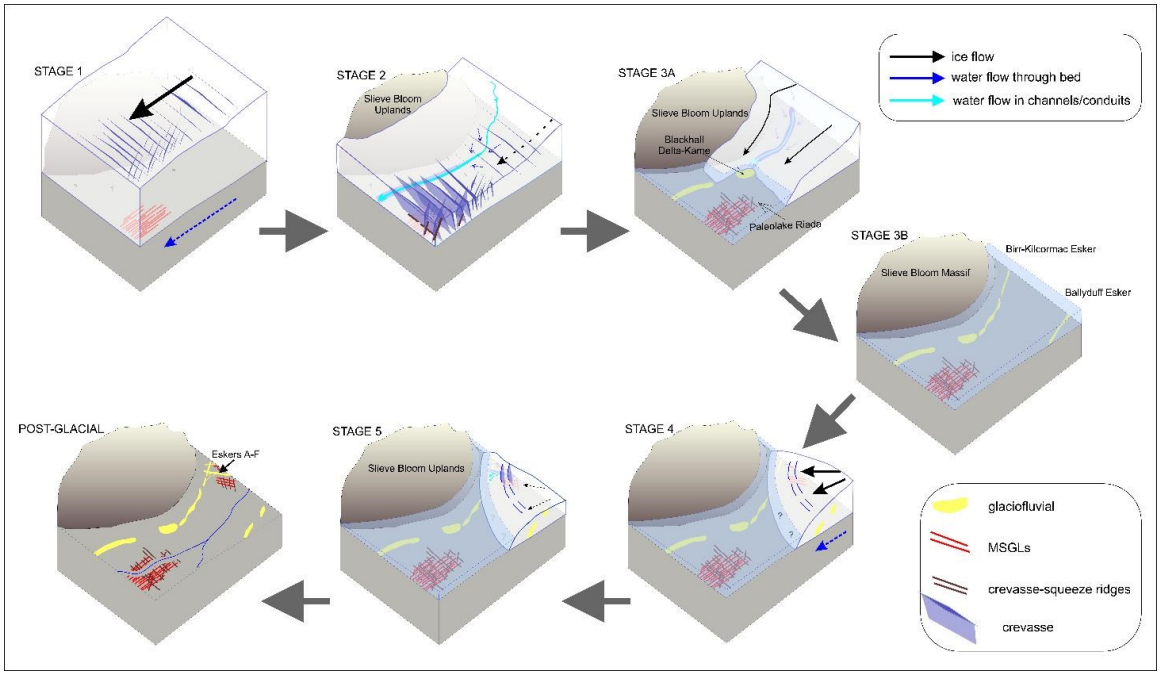
STAGE 1
STAGE 2
Slieve Bloom Uplands
STAGE 3A
Slieve Bloom Uplands
Blackhall Delta-Kame
Palealake Riada
ice flow
water flow through bed
water flow in channels/conduits
STAGE 3B
Slieve Bloom Massif
Birr-Kilcormac Esker
Ballyduff Esker
STAGE 4
STAGE 5
Slieve Bloom Uplands
POST-GLACIAL
Eskers A-F
glaciofluvial
MSGLs
crevasse-squeeze ridges
crevasse

1057